

ОБЪЕДИНЕННЫЙ ИНСТИТУТ ЯДЕРНЫХ ИССЛЕДОВАНИЙ JOINT INSTITUTE FOR NUCLEAR RESEARCH

6[63]-93

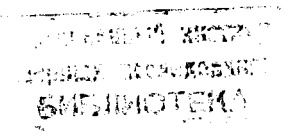
JINR RAPID COMMUNICATIONS

## Объединенный институт ядерных исследований Joint Institute for Nuclear Research

6[63]-93

# JINR RAPID COMMUNICATIONS

сборник collection



Дубна 1993

## ОГЛАВЛЕНИЕ CONTENTS

S.A.Avramenko, V.D.Aksinenko, M.Kh.Anikina, B.P.Bannik,
Yu.A.Belikov, V.A.Butenko, V.A.Drozdov, A.G.Galperin,
N.S.Glagoleva, A.I.Golokhvastov, N.I.Kaminsky, S.A.Khorozov,
E.V.Kozubsky, B.A.Kulakov, J.Lukstins, V.L.Lyuboshits,
O.Yu.Mandrik, P.K.Manyakov, A.T.Matyushin, V.T.Matyshin,
N.M.Nikityuk, L.S.Okhrimenko, O.V.Okhrimenko, T.G.Ostanevich,
V.B.Radomanov, P.A.Rukoyatkin, I.S.Saitov, S.A.Sedykh,
V.F.Zavyalov, V.P.Kondratiev, L.V.Krasnov, A.G.Semchenkov,
I.E.Shevchenko, I.V.Stepanov, K.Gajewski, J.Mirkowski,
Z.Pavlowski, A.Piatkowski, E.K.Khusainov, N.N.Nurgozhin,
Yu.S.Pol, G.G.Taran
Pion Momentum Spectra in a Nuclear Charge Exchange
Reaction $Mg(t, {}^{3}He)$
С.А.Авраменко, В.Д.Аксиненко, М.Х.Аникина,
Б.П.Банник, Ю.А.Беликов, В.А.Бутенко, В.А.Дроздов,
А.Г.Гальперин, Н.С.Глаголева, А.И.Голохвастов,
Н.И.Каминский, С.А.Хорозов, Э.В.Козубский,
Б.А.Кулаков, Ю.Лукстиньш, В.Л.Любошиц,
О.Ю.Мандрик, П.К.Маньяков, А.Т.Матюшин,
В.Т.Матюшин, Н.М.Никитюк, Л.С.Охрименко,
О.В.Охрименко, Т.Г.Останевич, В.Б.Радоманов,
П.А.Рукояткин, И.С.Саитов, С.А.Седых, В.Ф.Завьялов,
В.П.Кондратьев, Л.В.Краснов, А.Г.Семченко,
И.Е.Шевченко, И.В.Степанов, К.Гаевски, Я.Мирковски,
З.Павловски, А.Пиатковски, Е.К.Хусаинов,
Н.Н.Нургожин, Ю.С.Поль, Г.Г.Таран
Пионные спектры в реакции перезарядки ядер $Mg(t, {}^{3}He)$ 5
A.D.Kovalenko, V.A.Mikhailov, A.M.Taratin, E.N.Tsyganov
Design Concept and Computer Simulation
of Nuclotron Beam Extraction System with a Bent Crystal
А.Д.Коваленко, В.А.Михайлов, А.М.Таратин,
Э.Н.Цыганов
Концепция и компьютерное моделирование системы
вывода пучка из Нуклотрона изогнутым кристаллом

R.M.Santilli
Isotopic Lifting of SU(2)-Symmetry with Applications to Nuclear Physics
Р.М.Сантилли
Изотопическая $SU(2)$ -симметрия в применении к ядерной физике
A.V.Bakaev, V.I.Kabanovich
Solution to the One-Dimensional Cluster Model
А.В.Бакаев, В.И.Кабанович Решение одномерной кластерной модели
A.A. Vasil'ev, S.B. Vorozhtsov, V.P. Dmitrievsky, E.A. Myae, V.A. Teplyakov
Acceleration of Deuterons at the UNK (Proposal)
А.А.Васильев, С.Б.Ворожцов, В.П.Дмитриевский, Э.А.Мяэ, В.А.Тепляков
Ускорение дейтронов в УНК (Предложение)
M.Lewitowicz, R.Anne, G.Auger, D.Bazin, M.G.Saint-Laurent, R.Grzywacz, M.Pfützner, K.Rykaczewski, J.Zylicz, S.Lukyanov, A.Fomichov, Yu.Penionzhkevich, O.Tarasov, V.Borrel, D.Guiillemaud-Mueller, A.C.Mueller, H.Keller, O.Sorlin, F.Pougheon, M.Huyse, T.Pluym, J.Szerypo, J.Wauters, C.Borcea, K.Schmidt, Z.Janas
Experimental Study of Superneutron-Deficient Tin Isotopes
М.Левитович, Р.Анне, Г.Аугер, Д.Базен, М.Ж.Сант-Лоран, Р.Грживач, М.Пфитцнер, К.Рыкашевски, Я.Жилич, С.Лукьяног, А.Фомичев, Ю.Пенионжкевич, О.Тарасов, В.Боррел, Д.Гиймо-Мюллер, А.С.Мюллер, Х.Келлер, О.Сорлен, Ф.Пужо, М.Хойз, Т.Плюм, Я.Шерипо, Ж.Уотерс, К.Борча, К.Шмидт, З.Янас
Эксперименты по синтезу супернейтронодефицитных

# PION MOMENTUM SPECTRA IN A NUCLEAR CHARGE EXCHANGE REACTION Mg(1, <sup>3</sup>He)

S.A.Avramenko, V.D.Aksinenko, M.Kh.Anikina, B.P.Bannik, Yu.A.Belikov, V.A.Butenko, V.A.Drozdov, A.G.Galperin, N.S.Glagoleva, A.I.Golokhvastov, N.I.Kaminsky, S.A.Khorozov E.V.Kozubsky, B.A.Kulakov, J.Lukstins, V.L.Lyuboshits, O.Yu.Mandrik, P.K.Manyakov, A.T.Matyushin, V.T.Matyshin, N.M.Nikityuk, L.S.Okhrimenko, O.V.Okhrimenko, T.G.Ostanevich, V.B.Radomanov, P.A.Rukoyatkin, I.S.Saitov, S.A.Sedykh, V.F.Zavyalov Joint Institut for Nuclear Research, 141980, Dubna, Moscow Region, Russia

V.P.Kondratiev, L.V.Krasnov, A.G.Semchenkov, I.E.Shevchenko, I.V.Stepanov St.Petersburg State University, St.Petersburg, Russia

K.Gajewski, J.Mirkowski, Z.Pavlowski, A.Piatkowski Radiotechnical Institute, Warsaw University, Warsaw, Poland

E.K.Khusainov, N.N.Nurgozhin HEPI Kaz.AS, Alma-Ata, Kazakhstan

Yu.S.Pol, G.G.Taran Lebedev Institute of Physics, RAS, Moscow, Russia

The charge exchange reaction  $Mg(t, ^3He)$  was investigated in an experiment using a streamer chamber. The branching ratios of the reaction channels (topologies) were obtained. The experimental momentum spectrum for pior s was compared with the calculated one, and only 50% of pions were shown to be emitted by the delta isobars produced on a quasi-free nucleon in the arget nucleus. It was also found that the mass of delta incorporated in the nuclei s was reduced by 30-50 MeV in comparison with a free delta.

The investigation has been performed at the Laboratory of High Energies, JINR.

## Пионные спектры в реакции перезарядки ядер $Mg(t, {}^{3}He)$

#### С.А. Авраменко и др.

Ренкция перезарядки Mg (t, <sup>3</sup>He) исследована в стримерной камере. Определены соотношения вероятностей каналов реакций (топологий). Экспериментальный импульсный спектр пионов сравнивался с расчетными, что позволило установить, что только 50% пионов могут быть рождены при возбуждении дельта-изобары на квазисвободном нуклоне в ядре мишени. Выяснилось также, что масса связанной в ядре дельта-изобары на 30--50 МэВ меньше массы свободной изобары.

Работа выполнена в Лаборатории высоких энергий ОИЯИ.

Numerous investigations of the inclusive cross sections in charge exchange reactions ( ${}^{3}$ He, t) at various energies and targets have shown [1,2] a significant role of isobar excitation in the process. It was also observed that the  $\Delta$  peak in the t energy spectrum was broader and shifted towards a high energy region in the case of nuclear targets as compared with charge exchange on hydrogen. Collective effects like deexcitation of delta via the nonmesonic channel [3,4]  $\Delta N \rightarrow NN$  or coherent pion production [5,6,7] in the target nucleus, suggested as well as the excitation of the isobar in the projectile nucleus [8], were discussed to explain the observed features.

To fine out the predicted channels, the charged particles produced in the charge exchange reactions were registered and measured by large acceptance spectrometers in KEK [9], Dubna [10,11] and Saturne [12] experiments. In this way significant information about the role of collective effects like nonmesonic discharge of the delta isobar  $\Delta N \rightarrow NN$  was obtained. The coherent pion production observed in the recent experiment [13] has confirmed that the approach is fruitful.

However, for a clear theoretical interpretation of the charge exchange reactions and delta interactions in nuclei, it is necessary to find out all involved processes and to measure the branching ratios of these processes. Our experiment was devoted mainly to this problem because the streamer chamber is really a  $4\pi$  detector and the corrections due to the efficiency of trigger and chamber sensitivity are quite small. Therefore the reaction channels can be specified according to the number of produced charged particles with a subsequent detailed analysis of the channels. Particularly in this work the pions produced via delta excitation in the target nucleus were searched and the energy of nondelta pions was shown to be rather high. In other words, the analysis was devoted to the investigation of the channel with a single pion where the delta dominance was expected and a large nondelta fraction was rather a surprise.

The experiment was performed using the GIBS spectrometer facility in a 9 GeV/c tritium beam. The details of the experiment were discussed in the previous papers [10,11]. Here we would like to remind of a short list of the event measuring accuracy available in the analysis. The momenta of secondary charged particles were measured for all the events. The typical measuring accuracy of momentum was 2-3% for  $^3$ He nuclei and 1-2% for  $\pi^-$  and protons. The angles were measured with an error equal approximately to a few milliradians.

All positive secondary particles were regarded as protons, and negative particles, as  $\pi^-$ . The admixture of electrons (positrons) from  $\gamma$  conversion in the target did not exceed a few per cent of the total number of charged particles produced in the reaction. Nevertheless, almost all these leptons were excluded from the analysis because they were identified by ionization. Naturally, there was no doubt to identify the <sup>3</sup>He track: besides the ionization criterion, the <sup>3</sup>He momentum should be inside the specified band quite different from that expected for possible background tracks of p or d. The <sup>3</sup>He trajectories were extrapolated to the position of the trigger counters to check whether the chamber was triggered by the measured nucleus.

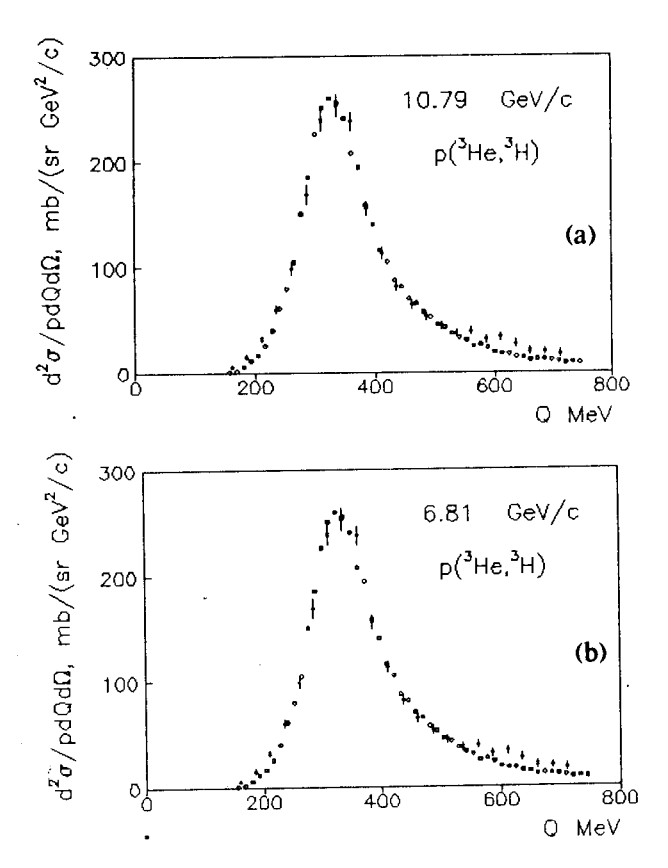
The total number of the identified and analyzed events was 1861. The numbers  $(N_{-})$  of  $\pi^{-}$  and  $(N_{+})$  of protons produced in the interaction were used to specify different channels of the reaction. Quasi-elastic interactions are not the subject of this experiment therefore the data from [3,14] were used to estimate (see also [11]) the fraction of quasi-elastic charge exchanges  $(0.12\pm0.01$  of the total number of events) and to reduce the number of events in the group  $(N_{-}=0, N_{+}=0)$  by 223. The reduced total number, 1638, was used to normalize the topological cross sections

presented in the Table. (The cross sections of charge exchange reactions were presented in our previous paper [11].) It should be noted that small corrections like absorption of slow protons in the target were not taken into account in the Table.

One can see in the Table that the channel (1,0) is the most intensive and the only one that can be practically observed in the case of delta production on a quasi-free target nucleon. Now there is a natural idea to calculate the momentum spectrum for pions produced by deexcitation of delta and to compare the calculated distribution with the

Table of the rormalized topological cross sections: R — fraction of events with specified topology (N\_, N\_)

N_	N <sub>+</sub>	R
0	0	0.32±0.015
1	0	$0.38 \pm 0.016$
1	1	$0.089 \pm 0.008$
0	1	0.14±0.01
0	2	$0.035 \pm 0.005$
other		0.036



Figs.1a and 1 b. Delta production model test. Points o in (a) and (b) calculated for two beam momentum values;  $\bullet$  — experimental data [16]. The calculated spectra normalized at the maximum value. Q — energy, transferred to the target

experimental one. Our calculation is based on the assumption that delta production on the free and quasi-free nucleon should be similar and the same model can be used as in the case of *NN* interactions.

At first we had to check the model and calculation procedure itself by comparing with the experimental data. To describe delta production in NN interactions, we have used the same formulae and parameters as Jackson [15]:

$$W(\omega) = \frac{\omega_0 \Gamma(\omega)}{0.898\pi \left[ (\omega^2 - \omega_0^2)^2 + \omega_0^2 \Gamma^2(\omega) \right]};$$

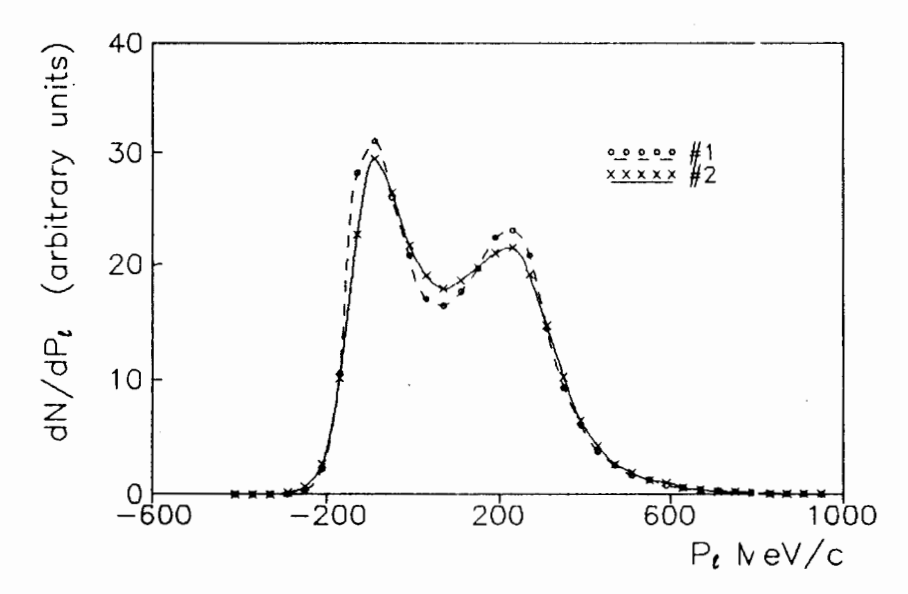


Fig.2. Pion longitudinal momentum calculated for the delta production on: a free nucleon (#1); a quasi-free target nucleon (#2)

$$\Gamma(\omega) = \Gamma_0 \left(\frac{q}{q_0}\right)^3 \frac{\rho(\omega)}{\rho(\omega_0)}; \ \rho(\omega) = [am_\pi^2 + q^2]^{-1};$$

$$a = 2.2$$
;  $\Gamma_0 = 123$  MeV;  $\omega_0 = 1232$  MeV.

These formulae provide the distribution  $W(\omega)$  of delta mass  $\omega$  and, subsequently, pion momentum q in the  $\Delta$  frame. Figures 1a and 1b show that the model is good enough to describe the experimental data [16] for the charge exchange reaction on hydrogen target  $p(^3\text{He}, t)$  at different projectile energies. It should be also emphasized that in our experiment the beam energy was intermediate (9.15 GeV/c) in comparison with these two reference energies [16]. The same form factor was used here as ir [16,17].

The next step in the calculation process was the introduction of nuclear (target) medium effects. One should expect a serious problem how to choose the distribution of Fermi momentum and binding energy for a target nucleon. Figure 2 shows that the pion momentum spectrum is rather insensitive to this choice. Indeed, one can see that two curves are much alike. One of them represents the pion longitudinal momentum distribution calculated in the case of the delta produced on a free nucleon. The second curve is for the delta produced on a quasi-free target nucleon on the

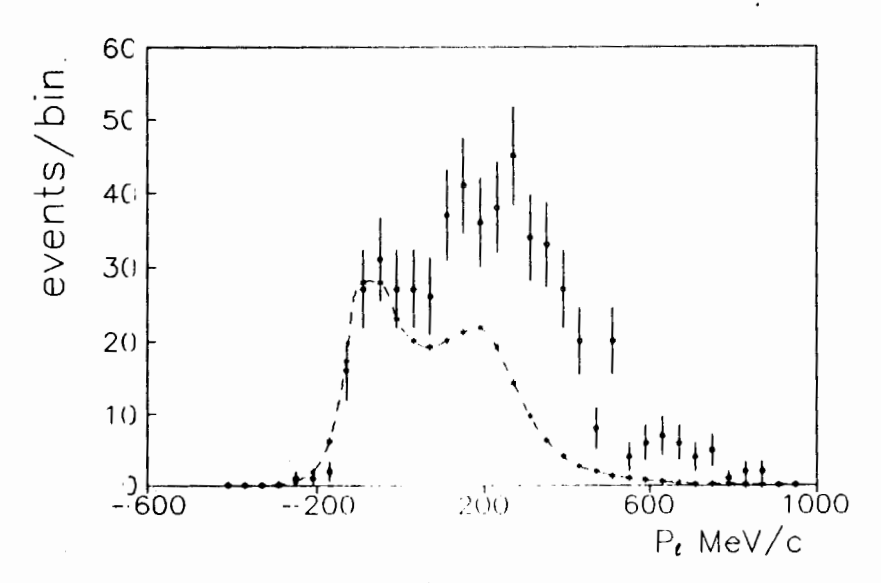


Fig. 3. o — pion longitudinal momentum  $(P_n^l)$  spectrum (#1 — experiment). x — pion spectrum (#2) calculated for  $\Delta$  produced on a quasi-free nucleon. The value of  $\Delta$  mass reduced to 190 MeV. The calculated spectrum was normalized so that it might not exceed the experimental data in any region of the spectrum

assumption of the Fermi momentum distribution like  $P^2dP$  over a 0—200 MeV/c interval (slightly less than in [18]) and a separation energy equal to  $E_{s,p}=20$  MeV (evaluated from [19]). If the two curves are very similar, there cannot be a strong dependence either on the value of  $E_{sep}$  or on the Fermi momentum parameters. The additional calculation has proved that the pion momentum spectrum should be independent of the beam momentum distribution. It is worthy of note that such a projectile momentum independence was predicted in [8] for the delta produced in the target contrary to delta production in the projectile. Considering the two peaks in the pion spectrum, it should be noted that they arise from the angular distribution  $1+3\cos^2\Theta$  which is essential in the OPE model.

All these tests were performed before the comparison of our experimental data and the calculated pion spectrum (see Fig.3). It is clear that only some part of real events can be produced in the process of delta excitation on a quasi-free target nuclon. In addition, it should be stressed that a possible improvement of the calculation procedure (more careful choice of parameters) cannot change this result significantly. Indeed, the calculated spectrum is centered with the value of  $\Delta$  mass, but the left side is

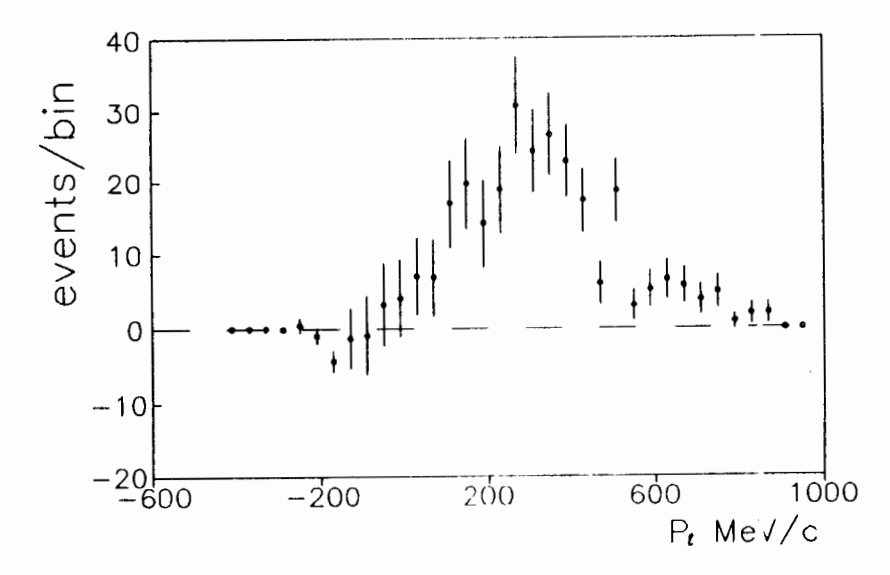


Fig. 4. The spectrum of nondelta pions obtained by subtraction of the spectrum (#2) (model) from the spectrum (#1) (experiment); see Fig. 3

fixed with the experimental spectrum. Moreover, to improve the left-side fit we had to reduce the delta mass by 40 MeV in comparison with the free delta. But if the delta mass decreases then the width of the pion momentum distribution becomes slightly narrow. (The reduction of the celta mass approximately by the same value of 30 MeV was observed in the Saturne [12] and KEK [9] experiments.)

Finally, we have obtained that 50% of the events are beyond the delta isobar spectrum, see Fig.3. The momentum distribution of these nondelta pions is reproduced in Fig.4. Here the mean value of longitudinal momentum  $\langle P_{\pi}^{l} \rangle = 360 \text{ MeV/c}$  is substantially higher than for delta pions, where  $\langle P_{\pi}^{l} \rangle = 90 \text{ MeV/c}$ .

The topological cross sections of the charge exchange reaction  $Mg(t, ^3He)$  were measured in real  $4\pi$  geometry when minimum corrections for the branching ratios were needed.

The longitudinal momenta of pions were analyzed and it was settled that only 50% of the pions observed in the reaction  $t + \text{Mg} \rightarrow {}^{3}\text{He} + \pi^{-} + \dots$  can be described by the momentum spectrum calculated in the frame of the model with the delta produced on a quasi-free target nucleon. The mean momentum for the pions outside the calculated

spectrum was much higher than that expected in the case of isobar decay. The production mechanism of these high energy pions should be investigated in future analysis and experiments.

There is evidence that the mass of delta isobar embedded in the Mg nucleus is recuced by the value of 30—50 MeV like a binding energy.

We are thankful to F.Gareev, E.Oset, M.Podgoretsky, Yu.Ratis, E.Strokovsky and L.Strunov for encouraging discussions and fruitful remarks. This work was supported in part by the Russian Fundamental Research Founcation (93-2-3908).

#### Refererces

- 1. Ableev V.G. et al. Pis'ma v ZhETF, 1984, 40, p.35, JETP Lett, 1984, 40, p.763.
- 2. Contardo D. et al. Phys. Lett., 1986, B168, p.331.
- 3. Ableev V.G. et al. Yad. Fiz., 1991, 53, p.457.
- 4. Gareev F.A., Ratis Yu.L. JINR E2-89-876, Dubna, 1989; Ratis Yu.L., et al. — Scient. Techn. Report 1991-11, Bergen, 1991.
- 5. Chanfray G., Ericson M. Phys. Lett., 1984, B141, p.163.
- 6. Delorme J., Guichon P.A.M. Phys. Lett., 1991, B263, p.157.
- 7. Udagava T.U., Hong S.-W., Osterfeld F. Phys. Lett., 1990, B245, p.1; Phys. Lett., 1993, B299, p.194.
- Oset E., Shiino E., Toki H. Phys. Lett., 1989, B224, p.249;
   Fernances de Cordoba P., Oset E. Preprint IFIC/92-8-FTUV/92-8,
   Burjassot, 1992.
- 9. Chiba J. et al. Phys. Rev. Lett., 1991, 67, p.1982.
- Avrame iko S.A et al. JINR P1-91-240, Dubna, 1991, see also Strokovsky E.A. et al. Int. Workshop on Pions in Nuclei, Penyscola, Spain, 991, «Pions in Nuclei», ed. E.Oset and M.J.Vicente Vacas, World Scientific, 1992, pp.395—405.
- 11. Avramenko S.A. et al. JINR Rapid Commun., No.3[54]-92, Dubna, 1992, p. 13.
- 12. Hennin T. et al. Nuclear Phys., 1991, A 527, p.399.
- 13. Hennino T. et al. Phys. Lett., 1993, B303, p.236.
- 14. Ableev V.G. et al. Yad. Fiz., 1988, 48, p.27.
- 15. Jackson J.D. Nuovo Cim., 1964, 34, p.1644.
- 16. Ableev V.G. et al. Yad. Fiz., 1987, 46, p.549.
- 17. Dunn P.C. et al. Phys. Rev., 1983, C27, p.71.
- 18. Monitz E.J. et al. Phys. Rev. Lett., 1971, 26, p.445.
- 19. Arditi et al. Nucl. Phys., 1967, A103, p.319.

# DESIGN CONCEPT AND COMPUTER SIMULATION OF NUCLOTRON BEAM EXTRACTION SYSTEM WITH A BENT CRYSTAL

#### A.D.Kovalenko, V.A.Mikhailov, A.M.Taratin, E.N.Tsyganov

The scheme of nuclei beam extraction from Nuclotron by means of a bent crystal has been considered. Different methods for the beam guidance ont) the crystal were discussed. It is more reasonable to simultaneously use an orbit tump and a transverse diffusion of the beam particles. Deflection efficiency of the nuclei beam with energy of 6 GeV/u by a bent silicon crystal and their mult turn extraction from Nuclotron has been studied by computer simulation. It was shown that with an optimal crystal length the extraction efficiency may be increased considerably due to multiple passages of particles through the crystal deflector.

The investigation has been performed at the Laboratory of High Energies, JINR.

# Концепция и компьютерное моделирование системы вывода пучка из Нуклотрона изогнутым кристаллом

## А.Д.Коваленко, В.А.Михайлов, А.М.Таратин, Э.Н.Цыганов

Рассмотрена схема использования изогнутого кристалла для выгода пучка релятивистских ядер из Нуклотрона. Дан анализ различных методов наведения частиц на дефлектор. Показана целесообразность использования одновременно локального искажения орбиты и поперечной диф рузии частиц. Компьютерным моделированием исследована эффективне сть отклонения ядер с энергией 6 ГэВ/нуклон изогнутым монокристаллом кремния и многооборотный вывод их из Нуклотрона. Показано, что при оптимальной длине кристалла эффективность вывода пучка можут б эть значительно увеличена за счет кратных прохождений частиц через к зисталлический дефлектор.

Работа выполнена в Лаборатории высоких энергий ОИЯИ.

#### 1. Introduction

The first beam extraction from a cyclic accelerator by means of a bent crystal was performed at the Dubna synchrophasotron [1] and then at the IHEP synchrotron [2]. In both the cases the extraction efficiency was small enough, about 10<sup>-4</sup>, because the systems used for the beam guidance were

not optimal. So, a fast decreasing of the closed orbit radius was used at the synchrophasiotron and the orbit bump at the IHEP synchrotron.

The crystal deflectors have good perspectives of usage for particle extraction from a beam halo at the largest proton and ion colliders SSC, LHC, RHIC and UNC. The most attractive feature of such an extraction is that the colliding mode of machine operation is not disturbed, and some fixed target experiments may be carried out simultaneously. The experimental study of appropriate extraction systems for SSC and LHC are under investigation now at the Tevatron and the SPS [3,4]. So, a successful extraction of 20 GeV proton beam from the SPS with a record efficiency of about 10% was fulfilled recently at CERN [5]. The injection of a white noise at the deflector plates of the feedback system was used to initiate the transverse (liffusion of particles onto the bent crystal. On the other hand, a longitudinal diffusion of beam halo particles onto the crystal was proposed for the SSC beam extraction [6]. Moreover, a resonance method for increasing the longitudinal oscillations of beam halo particles without perturbation of the beam was offered by the authors [7].

The extraction efficiency of the beam from a cyclic accelerator  $P_{ex}$  may be higher than a beam deflection efficiency by a bent crystal due to multiple passages of the beam particles through the crystal [8,9]. It occurs when the crystal length is not large, so  $S_{cr} < S_{ms}$  and  $S_{cr} < S_n$ , where  $S_{ms}$  is the length through which the rms angle of multiple scattering becomes equal to the channeling critical angle  $\theta_c$ , and  $S_n$  is the nuclear interaction length of the crystal. The first condition determines the growth rate of the beam divergence due to multiple scattering in the crystal; the second one, decreasing of the circulating beam intensity.

In this work the analytical estimations and computer simulation of the nuclei deflection efficiency were fulfilled for JINR Nuclotron, at which the first results with the beam accelerating have been received recently [10,11]. It is necessary to locate the crystal deflector at the azimuth, where the beam divergence is maximum, and the beam envelope is far from the closed orbit. That is, near a focusing quadrupole. A necessary angle of deflection by the crystal is about 50 mrad for Nuclotron to go out a next defocusing quadrupole. The cryogenic equipments are the obstacles for the extraction in a horizontal direction. Therefore, the extraction in a vertical direction is considered here. Figure 1 shows the scheme for the beam extraction from Nuclotron The possibilities for the Nuclotron beam guidance onto the crytal deflector either by means of the closed orbit bump, which may be created by the existing system of correcting magnets, or as the result of a transverse diffusion initiated due to a noise injection into the inflector plates, have been studied by computer simulation. It was shown, that for

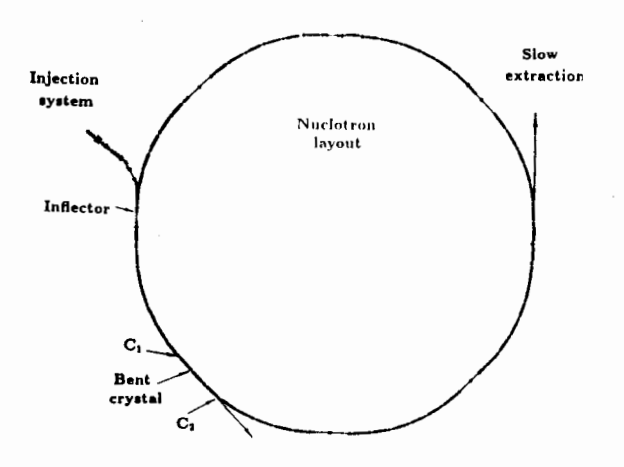


Fig.1. Nuclotron layout with the elements for the beam extraction by means of a bent crystal: inflector,  $C_1$ ,  $C_2$  — correcting coils, bent crystal

Nuclotron in the case of the maximum particle energy the extraction efficiency may be increased considerably due to multiple passages of the circulating beam particles through the deflector.

### 2. Beam Deflection Efficiency by a Bent Crystal

1. Dependence on  $\omega=A/Z$ . Let us consider according to [12] the change of the main characteristics of particle channeling in a bent crystal in going from protons to nuclei (Z,A) with the same energy per nucleon  $E_1$ , and estimate for Nuclotron the crystal deflector efficiency with a maximum particle energy. The critical bend radius of the crystal  $R_c$ , at which the particle channeling is possible yet, is proportional with  $\omega$ 

$$R_c^{\omega}(E_1) = \omega R_c^{\dagger}(E_1). \tag{1}$$

If the bend is measured in the relative units,  $r = R/R_c$ , then a critical angle of the particle direction with the atomic planes of the crystal for channeling decreases with  $\omega$ 

$$\vartheta_c^{\omega}(r; E_1) = \omega^{-1/2} \vartheta_c^1(r; E_1).$$
 (2)

Suppose also that the rms beam divergence is measured in the relative units,  $k = \theta_x/\theta_c$ , then at the same crystal bend r, the particle capture into the channeling states does not depend upon  $\omega$ 

$$P_c^{\omega}(r, k; E_1) = P_c^{1}(r, k; E_1),$$
 (3)

and the dechanneling length increases proportionally with  $\omega$ 

$$S_d^{\omega}(r, k; E_1) \cong \omega S_d^{1}(r, k; E_1). \tag{4}$$

So, the beam deflection efficiency by a bent crystal at a required angle  $\alpha$  does not depend on  $\omega$  also at the same r and k

$$P_d^{\omega}(\alpha; r, k; E_1) = P_d^{1}(\alpha; r, k; E_1),$$
 (5)

$$P_d^{1}(\alpha; r, k; E_1) = P_c^{1}(r, k; E_1) \exp\left[-\alpha \, r R_c^{1} / S_{1/e}^{1}(r, k; E_1)\right]. \tag{6}$$

By the other words in going from protons to nuclei with the same energy per nucleon,  $E_1$ , he crystal efficiency for the beam deflection remains without changing for the nuclei beam with divergence which is smaller  $\omega^{1/2}$  times than for the protons, and when a curvature of the crystal used is smaller  $\omega$  times.

2. Optimal dimensions and bend of the crystal deflector. The efficiency of deflection by a bent crystal is maximum for a parallel particle beam. For this case Fig. ?! shows the dependence of the deflection efficiency at the angle  $\alpha = 50$  mrad for protons, and nuclei of  ${}^6\mathrm{C}^{12}$  and  ${}^{79}\mathrm{Au}^{197}$  with energy 6 GeV/u upon the bend radius of the silicon crystal bent along (110) planes. It reaches about 20% in a maximum. The corresponding dependences of the dechanneling lengths are shown in Fig.3. These results were recieved by computer simulation of the beam passage through the crystal in the frame of the model with the averaged potential of the bent crystal planes, and with taking into account the change of the particle transverse energy due to multiple scattering by the crystal electrons and nuclei [13]. The dependences shown for the deflection efficiency differ by the scale of R. They are close to each other when the crystal bend is measured in the relative units r. that confirms our theoretical conclusions. The crirical radii of the crystal bend  $R_c^{\dot{\omega}}$  equals 1.16, 2.32 and 2.88 cm for the protons, nuclei C and Au, respectively. The optimal bend radius of the silicon crystal at which the beam deflect on efficiency is maximum for the nuclei beam extraction from Nuclotron is about 20 cm. The corresponding length of the crystal is 1 cm.

The considered deflection efficiencies of nuclei beams are maximum which may be recived. In reality, the particle beams have some divergence. The probability of the particle capture into the channeling regime at the entrance into the crystal and their dechanneling lengths decrease when the beam devergence increases. So, when the beam divergence equals the

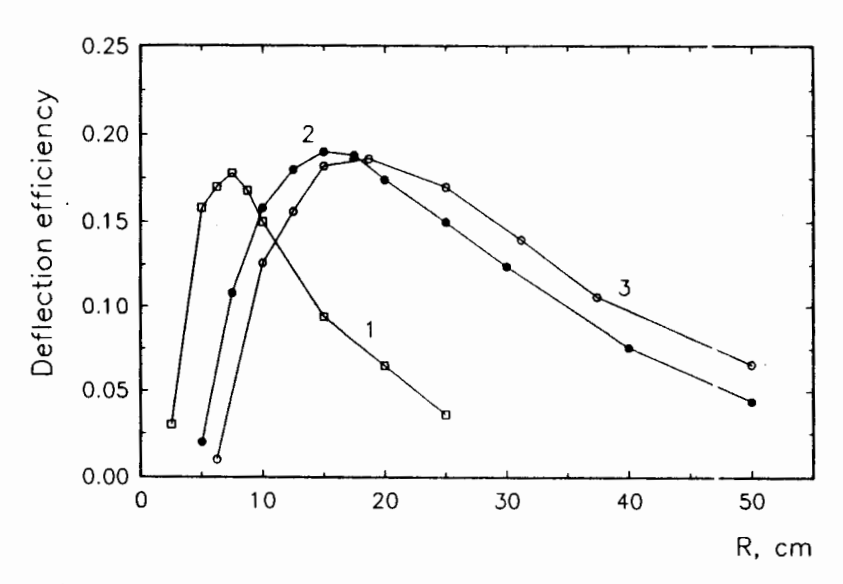


Fig. 2. The deflection efficiency of the parallel nuclei beam with energy 6 GeV/u by a silicon crystal bent along (110) planes as a function of the crystal bend radius R. The crystal bending angle 50 mrad. Curves: 1 — protons, 2 —  $^6C^{12}$ , 3 —  $^{79}Au^{197}$ 

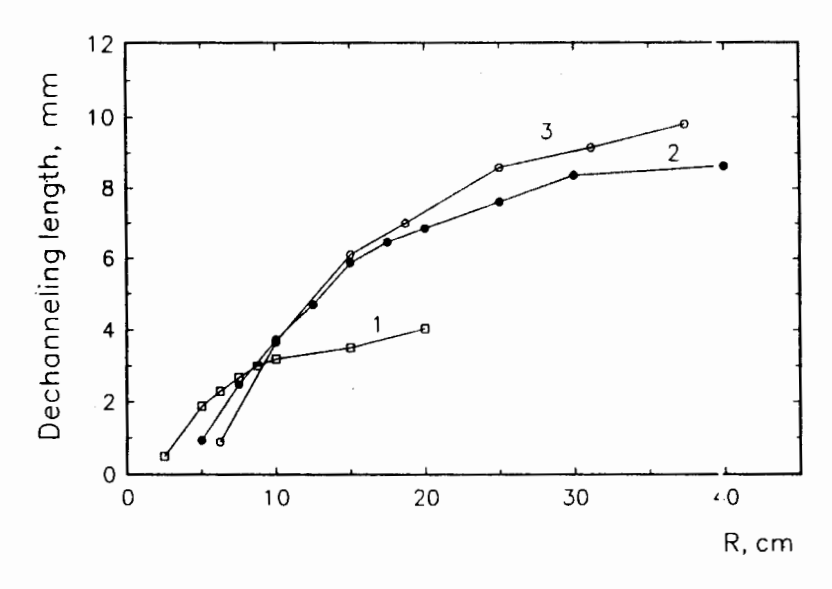


Fig.3. The nuclei dechanneling length as a function of the crystal bend radius. The conditions are the same as for Fig.2

critical channeling angle  $\theta_c$ , that is close to the value expected for Nuclotron at the beam guidance onto the crystal by a combination method (see below), the capture probability  $P_c$  and the dechanneling length  $S_d$  decrease two times. As a result the beam deflection efficiency at the considered angle of 50 mrad decreases approximately by an order of value.

The space acceptance of the crystal deflector, which is determined by its transverse dimensions, depends on its bend radius R. The point is that the perfect silicon and germanium crystals usually used in the channeling experiments may be elastically bent up to the definite limit after which they will be broken. This radius is proportional to the thickness of the crystal plate t. In the first experiment there was studied the beam deflection by a bent crystal, which was fulfiled in Dubna [14], it was shown that for a silicon crystal bent along (111) planes  $R_{br}$  (cm)  $\approx 76 \times t$  (mm). So, in our case for the realization of the optimal bend with R = 20 cm the crystal thickness has not to be more than 0.3 mm. The deflector width may be varied. When the width is 10 mm it is enough to overlap the beam. However, it may be profitable to have a more narrow deflector to increase the distribution width of particles in the vertical coordinate at the entrance into the deflector due to initial misses at the beam broadening.

So, the optimal dimensions of the silicon deflector for the beam extraction from Nuclotron are 10x10x0.3 mm. The usage of the crystals with the length about 2—6 cm is more usual. However, in our case increasing of the crystal length up to 2 cm will decrease the deflection efficiency about three times. Moreover, for nuclei it will decrease considerably the extraction possibility due to multiple passages through the deflector.

As it was marked, due to multiple passages through the deflector the extraction efficiency  $P_{ex}$  is higher than the deflection efficiency  $P_d$  for the beam with the same divergence. The maximum of  $P_{ex}$  shifts to a smaller bend radius to compare with  $P_d$  [8]. It means that the usage of a shorter crystal is more profitable. However, in our case the crystal length selected according to the condition that  $P_d$  is maximum is small enough to decrease it more.

### 3. Beam Guidance onto the Crystal

1. Orbit bump. A slow uniform shift of the beam onto the crystal by means of the closed orbit bump gives possibility for the beam particles to enter the planar crystal channels with very small angles. However, in this case «inpact parameters» are very small too. It means that these particles will move through the crystal in a narrow surface region. Therefore, they

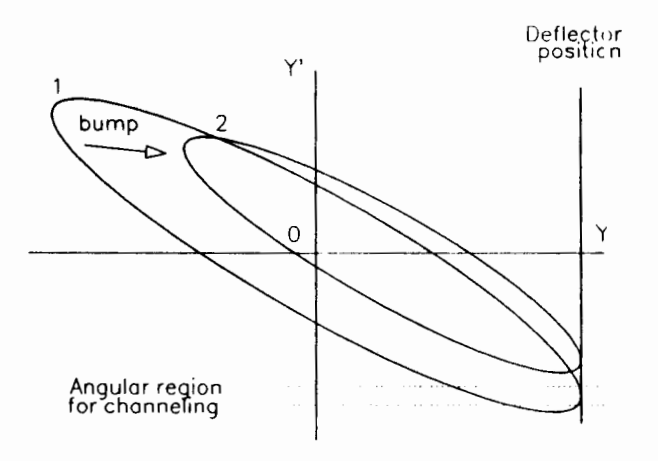


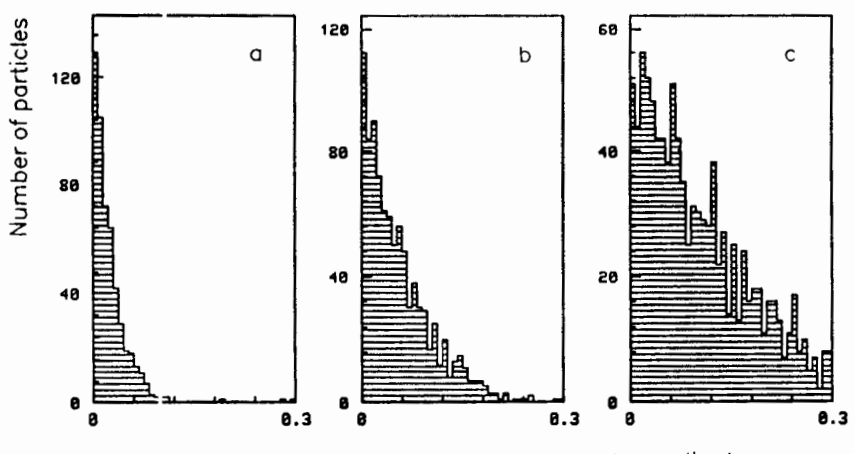
Fig. 4. Schematic picture of growing orbit bump which takes away the beam from the angular region of the capture into the channeling states in the bent crystal

will not deflect at the first hits with the deflector when there is an imperfection of the surface layer or the crystal surface is not parallel with the considered atomic planes.

Besides, there is another circumstance which appears at the bump usage. The deflector location near the center of the focusing quadrupole leads to large troubles with the crystal alignment while it is possible. On the outher side when it is located outside the quadrupole the growing orbit bump takes away the beam fast from the angular region of the capture into the channeling states, that is shown in Fig. 4.

Increasing of the betatron oscillations of the beam particles may be used for their guidance onto the deflector. It may be made by means of either the transverse diffusion initiated due to the noise injection on the inflector plates or the resonance excitation of these particles at the frequencies to which a rotation frequency  $f_0$  and the betatron oscillation one  $qf_0$  are multiple.

2. Transverse diffusion. Resonance excitation. The crystal deflector has to be located at the distance about 3 cm from the closed orbit to be not the obstacle for the beam particles at the injection stage. The rms particle distance from the closed orbit at the crystal assimuth is  $\sigma_{y0} = 0.5 \sqrt{\varepsilon_{y0} \cdot \beta_y} \cong 2.5$  mm, when the vertical emittance of the nuclei accelerated up to 6 GeV/u is  $\varepsilon_y = 2 \times 10^{-6}$ . Assuming that the beam begins to touch with the deflector at  $3\sigma_y$ , it means that the beam emittance has to be



Vertical coordinate, mm

Fig. 5. Transverse diffusion. The particle distributions in a vertical coordinate at the entrance into the crystal for the different values of the rms angular deviations received at their passage brough the inflector  $\sigma_{noi}$ ,  $\mu$ rad: 1 (a), 2.5 (b), 5 (c). The full crystal thickness is 0.3 mm

increased sixteen times to beging the extraction process. This beam broadening leads to the unprofitable increase of the angular divergence of the particles entering the crystal. The rms deflection angle of the beam particles at the passage through the inflector plates to have the required extraction du ation  $\tau$  may be estimated as

$$\sigma_{noi} = \sqrt{\frac{\Delta \, \varepsilon_y T_0}{\beta_y \tau}}.\tag{7}$$

So for  $\tau=1$  s it will be necessary to have  $\sigma_{noi}=1.5~\mu \rm rad$ . The rms voltage at the inflector plates equals respectively  $\langle~U~\rangle=0.6~\rm kV$  for the nuclei with energy 6 GeV/u and  $\omega=2$ .

For the simulation of the beam extraction from the Nuclotron two points in the accelerator lattice were considered. The inflector is located in the first point, and the bent crystal in the second one near the defocusing quadrupole through the superperiod from the inflector. The initial beam distribution is given at the bent crystal position. It is generated according to Gaussian with the rms deviations the values of which are determined by the beam emittance. Two transfer matrices are used to transport the particles from the bent crystal to the inflector and back. When the particles pass through the inflector plates they acquire the chance angular deflections in a vertical

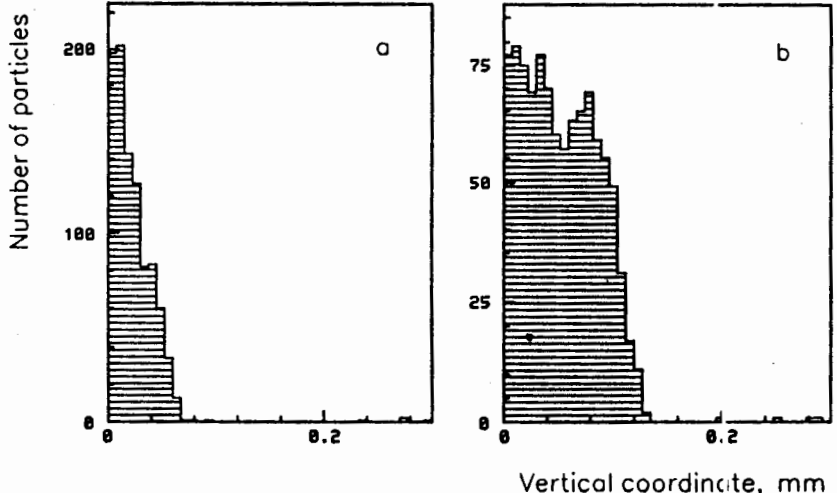


Fig.6. Resonance excitation. The particle distributions in a vertical coordinate at the entrance into the crystal. For the different angular deflections of the particles in the inflector  $\theta_{\nu}$ ,  $\mu$ rad: 5 (a), 10 (b). The period of the perturbations is  $T_{\nu} = 20 T_{0}$ 

direction. It causes their diffusion, and they begin to hit the crystal deflector.

Figure 5 shows the particle distributions in the vertical coordinate at the entrance into the crystal. They were calculated for the different values of the rms angular deviations received at the particle passages through the inflector. When  $\sigma_{noi} = 5 \mu \text{rad}$  the distribution width approximately equals the deflector thickness. With decreasing the noise value the width decreases.

The corresponding distributions when the resonance excitation of the beam particles was used are shown in Fig.6. The particle deflections in a vertical direction with the values of  $5 \mu rad$  (a)  $10 \mu rad$  (b) were realized at their passage of the inflector with the period  $T_{\nu} = 20 T_0$ . It was considered here with a vertical betatron tune  $q_v = 6.85$ . The distributions have a bellshape and are more narrow than in the case of the transverse diffusion with the same value of the rms angular deflections. Besides, the required time for the beam ejection onto the crystal is considerably smaller.

3. The combination method for the beam guidance. The multiturn beam extraction. So, the orbit bump takes away the beam from the angular region of the capture into the channeling states; on the other band, the beam broadening during the transverse diffusion decreases the deflection efficiency. Therefore, it will be more optimal to decrease the distance between the beam and the deflector by means of the bump up to the touching at  $3\sigma_{y0}$ , that is about 7 mm, and only then to throw the beam particles onto the deflector due to the transverse diffusion or the resonance excitation.

Assuming the usage of this method for the beam guidance onto the crystal the computer simulation of the Nuclotron beam extraction was fulfiled. The silicon crystal bent along (110) planes with the bending angle of 50 mrad has the optimal dimensions. The noise generator of the inflector begins to work when the beam approaches the crystal at the distance of 7 mm by means of the orbit bump. Some particles which enter the crystal may be lost due to the inelastic nuclear interactions. The mean path before the interactions for nuclei in the crystal  $S_n$  is proportional to  $A^{-0.71}$ . In the silicon it equals 45.5, 7.8 and 1.07 cm for protons, nuclei C and Au accordingly. The density of the other particle depends on the angle Y', which they have after the crystal passage. When  $Y' > \alpha - \theta_{col}$ , where  $\alpha$  is the bending angle,  $\theta_{col} = 100 \,\mu\text{rad}$  is a collimation angle, the particle will be extracted from the accelerator. The particles are lost downstream at the wall of the beam pipe when  $\theta_{ac} < Y' < \alpha - \theta_{cal}$ , where  $\theta_{ac} = 10$  mrad is the angular acceptance of Nuclotron. Otherwise the particles remain in the circulating beam.

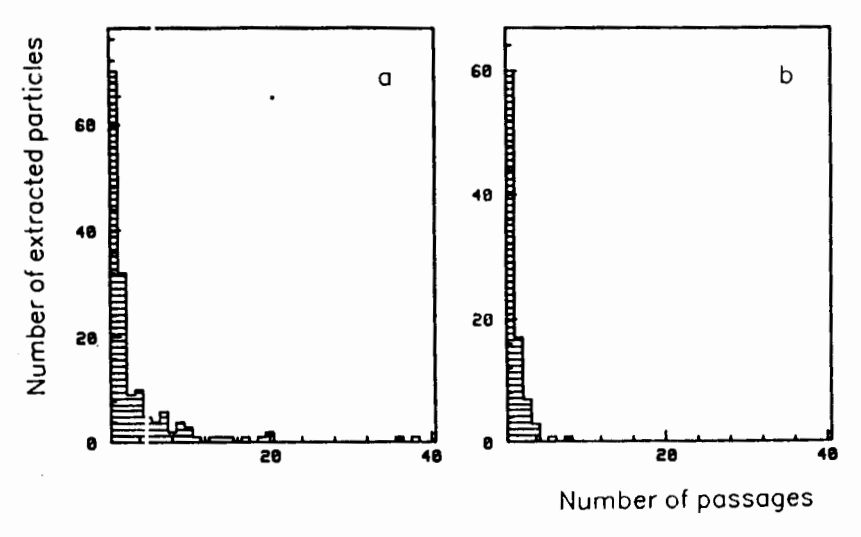


Fig. 7. The distributions of the extracted particles in the number of passage through the crystal before the extraction for the nuclei with energy 6 GeV/u: (a) -  $^6$ C<sup>12</sup>, (b) -  $^{79}$ Au<sup>197</sup>

The calculated extraction efficiency is more than 7% for nuclei of  ${}^6C^{12}$  and 4% for  ${}^{79}Au^{197}$ . The distributions of the extracted particles in the number of passages through the crystal before the extraction are shown in Fig.7 for nuclei C (a) and Au (b). The contribution of multiple passages increases significantly the extraction efficiency, which for the first hits with the crystal is only about 3% for both cases. The passage multiplicity is higher for nuclei of C, where it achieves 20, because the particle loss due to the nuclear interactions in the crystal is smaller for C than for Au. It is necessary to mark here that the extraction possibility due to multiple passages through the deflector may be considerably smaller for ions comparison with nuclei because their charge states may change at the first passage, and they may be lost from the circulating beam.

#### References

- Avdeichikov V.V. et al. JINR Rapid Communications 1-84, Dubna, 1984.
- 2. Aseev A.A., Bavizhev M.D. et al. Preprint IHEP 89-57, Serpukhov, 1989.
- 3. Carrigan R.A. et al. Proposal for a Test of Low Intensity Extraction from the Tevatron Using Channeling in a Bent Crystal, FNAL proposal P 853, 1991.
- 4. Jensen B.N. et al. A Proposal to Test Beam Extraction by Crystal Channeling at the SPS: a First Step Towards a LHC Extracted Beam, CERN/DRDC 91-25, 1991.
- 5. Akbari H. et al. Physics Letters, 1993, B313, p.491.
- 6. Shih H.-J., Taratin A.M. SSC Laboratory Report SSCL-339, March, 1991.
- 7. Taratin A.M., Tsyganov E.N., Shih H.-J. JINR Preprint E9-92-459, Dubna, 1992.
- 8. Taratin A.M. et al. Nucl. Instr. & Meth., 1991, B58, p.103.
- 9. Biryukov V.M. Nucl. Instr. & Meth., 1991, B53, p.202.
- 10. Baldin A.M. et al. JINR Preprint E9-93-273, Dubna, 1993.
- 11. Kovalenko A.D. In: Proc. on High Energy Physics, Merseille, July, 1993.
- 12. Kovalenko A.D., Taratin A.M., Tsyganov E.N. JINR Preprint E1-92-8, Dubna, 1992.
- 13. Taratin A.M., Vorobiev S.A. Nucl. Instr. & Meth., 1990, B47, p.247.
- 14. Elishev A.F. et al. Physics Letters, 1979, B88, p. 387.

Received on December 28,1993.

# ISOTOPIC LIFTING OF SU(2)-SYMMETRY WITH APPLICATIONS TO NUCLEAR PHYSICS<sup>1</sup>

#### R.M.Santilli23

We introduce the axiom-preserving, nonlinear, nonlocal and noncanonical isotopies/Q-operator deformations  $S\hat{U}_Q(2)$  of the SU(2)-symmetry; construct their isc representations; and prove their lack of unitary equivalence to conventional representations under the local isomorphism  $S\hat{U}_Q(2) \approx SU(2)$ . We then apply the theory to the reconstruction of the exact isospin symmetry under electromagnetic and weak interactions and to the exact representation of total magnetic moments for the deuteron and few-body nuclei under the exact isospin symmetry.

# Изотопическая SU(2)-симметрия в применении к ядерной физике

#### Р.М.Сантилли

Вводятся аксиомосохраняющиеся, нелинейные, нелокальные и неканонические изотопически/Q-операторные деформации  $SU_Q(2)$  SU(2)-симмет эии; создаются их изопредставления; и доказывается недостаток в них еди ной эквивалентности общепринятым представлениям в локальном изоморфизме  $\hat{SU}_Q(2) \approx SU(2)$ . Теория затем применяется к воссозданию точной изоспиновой симметрии в электромагнитных и слабых взаимодействиях 4 к точному представлению всех магнитных моментов дейтрона и малону слонной системы в точной изоспиновой симметрии.

#### 1. Statement of the Problem

It is generally assumed that the SU(2)-spin symmetry (see, e.g., [1]) can solely characterize the familiar eigenvalues j(j+1) and  $m, j = 0, \frac{1}{2}, ..., m = j, j-1, ..., -j$ .

In this note we shall show that the isotopic/Q-operator deformation of SU(2), herein denoted  $SU_Q(2)$ , while being locally isomorphic to SU(2), can characterize the more general eigenvalues

<sup>&</sup>lt;sup>1</sup>The article is suggested for discussion.

<sup>&</sup>lt;sup>2</sup>The Institute for Basic Research, Box 1477, Palm Harbor, FL 34682, USA,

$$J^{\widehat{2}} \Rightarrow f(\Delta)j \ [f(\Delta)j+1], \ J_3 \Rightarrow f(\Delta)m,$$
 (1.1)

and others, where j and m have conventional values and  $f(\Delta)$  is a real valued, positive-definite function of  $\Delta = \det Q$  such that f(1) = 1.

For the two-dimensional case, the condition  $\det Q=1$  for  $Q=\operatorname{diag}(g_{11},g_{22})$  is realized by  $g_{11}=g_{22}^{-1}=\lambda$ . This implies the preservation of the conventional value  $\frac{1}{2}$  of the spin, but the appearance of a non-trivial generalization of Pauli's matrices, herein called *isopculi matrices*, with an explicit realization of the «hidden variable»  $\lambda$  in the structure of the spin  $\frac{1}{2}$  itself.

As a first application, we construct the isotopies of the conventional isospin (see, e.g., [2,3]) and show that they permit the reconstruction of an exact  $S\widehat{U}(2)$ -isospin symmetry under electromagnetic and weak interactions because protons and neutrons acquire equal masses in the underlying isospace.

It should be noted that the isotopic lifting  $SU(2) \Rightarrow S\hat{U}_Q(2)$  can be interpreted as an application of the so-called q-deformations [4] although in their isotopic axiomatic formulation for the most general possible, integrodifferential operator Q [5].

In the recent note [6] we have presented the isotopies of Dirac's equation and shown their capability to provide a numerical representation of the magnetic moment of few-body nuclei. As a second application, in this note we re-inspect this result under an exact isospin symmetry realized with the same magnitude of the magnetic moments of protons and neutrons in isospace. Additional applications in nuclear physics, such as for the introduction of a small nonlocal-nonhamiltonian term in the nuclear force, will be presented elsewhere.

### 2. Isotopies of SU(2)-Symmetry

The understanding of this note requires a knowledge of: the nonlinear-nonlocal-noncanonical, axiom-preserving isotopies of Lie's theory, originally introduced in [7] (see the recent review [8] and general presentation [9]); the isotopies  $\hat{O}(3)$  of the rotational symmetry O(3) submitted in [10]; the isotopies  $\hat{O}(3.1)$  of the Lorentz symmetry O(3.1) submitted in [11]; and the isotopies of quantum mechanics (QM), called hadronic mechanics [HM], originally submitted in [12] and then elaborated by various authors (see recent studies [5,8,13] and monographs [14]).

The fundamental notion is the *isotopy of the unit* of the theory considered [5-14], in this case, the generalization of the conventional trivial unit I = diag (1, 1) of SU(2) into the most general possible, two-dimensional matrix  $\hat{I}$  preserving the original axioms of I (smoothness, boundedness, nonsingularity, Hermicity and positive-definiteness) as a necessary condition for isotopy.

$$I = \operatorname{diag}(1, 1) > 0 \Rightarrow \hat{I} = \hat{I}(t, z, \overline{z}, \dot{z}, \dot{z}\psi, \psi^{\dagger}, \partial\psi, \partial\psi^{\dagger}, \ldots) > 0.1 \quad (2.1)$$

The isotopy of the unit then demands, for consistency, a corresponding, compatible lifting of all associative products AB among generic QM quantities A, B, into the isoproduct

$$AB \Rightarrow A * B := AQB, \ O \text{ fixed},$$
 (2.2)

where the isotopic character of the lifting is established by the preservation of associativity, i.e., A \* (B \* C) = (A \* B) \* C.

The assumption  $\hat{I} = Q^{-1}$  then implies that  $\hat{I}$  is the correct left and right unit of the theory,  $\hat{I} * A = A * \hat{I} \equiv A$ , in which case Q is called the *isotopic element*, and  $\hat{I}$  is called the *isounit*. Note the appearance of q-deformations in their Q-operator form at the very foundation of the theory [5].

The isotopies of the unit  $I \Rightarrow \hat{I}$  and of the product  $AB \Rightarrow A * B$  then imply the necessary lifting of all mathematical structures of QM into those of HM [5—13]. Here we mention the lifting of the field of complex numbers C(x, +, x), with elements c, ordinary sum + and multiplication  $c \times c' = cc'$ , into the infinitely possible isotopies  $\hat{C}_Q(\hat{c}, +, *)$ , with isocomplex numbers  $\hat{c} = c\hat{I}$ , conventional sum + and isomultiplication  $\hat{c}_1 * \hat{c}_2 = \hat{c}_1 c \hat{c}_2 = \hat{c}_1 c \hat{c}_2$  (see [16,17] for details).

The isotopies of the unit, multiplication and fields then demand, for mathematica consistency, corresponding compatible isotopies of the basic carrier space, the two-dimensional complex Euclidean space  $E(z, \bar{z}, \delta, C)$  with familiar metric  $\delta = \text{diag}(1, 1)$  into the complex two-dimensional iso-euclidean spaces introduced in [11]

$$\hat{E}_{Q}(z, \overline{z}, \hat{\delta}, \hat{C}) : z = (z_{1}, z_{2}),$$

$$\hat{\delta} = Q\delta \equiv g = \operatorname{diag}(g_{11}, g_{22}) = g^{\dagger} > 0,$$
(2.3a)

$$z_i^{\dagger} g_{ij}(t, z, \overline{z}, ...) z_j = \overline{z}_1 g_{11} z_1 + \overline{z}_2 g_{22} z_2 = \text{inv.},$$
 (2.3b)

where the assumed diagonalization of Q is always possible (although not necessary) from its positive-definiteness.

The isotopic character (as well as novelty) of the generalization is established by the fact that, under the *joint* lifting of the metric  $\delta \Rightarrow \hat{\delta} = Q\delta = g$  and of the field  $C \Rightarrow \hat{C}_Q$ ,  $\hat{I} = Q^{-1}$ , all infinitely possible isospaces  $\hat{E}_Q(z, \overline{z}, \hat{\delta}, \hat{C})$  are locally isomorphic to the original space  $E(z, \overline{z}, \delta, C)$  under the condition of positive-definiteness of the isounit  $\hat{I}$  [11]. In turn, this evidently sets the foundation for the local isomorphism of the corresponding symmetries.

Note that separation (2.3) is the most general possible nonlinear, non-local and noncanonical generalization of the original separation  $z^{\dagger}z$  under the sole condition of remaining positive-definite, i.e., of preserving the topology sig  $\delta = \text{sig } \hat{\delta} = (+, +)$ . The symmetries of invariant (2.3) are then expected to be nonlinear, nonlocal and noncanonical, as desired.

The preceding isotopies imply, for consistency, the isotopies of Hilbert spaces  $(\psi \mid \varphi) \in C$  into the so-called isohilbert space Q with isoproduct and isonormalization

$$\widehat{Q}:\langle\widehat{\psi}\uparrow\widehat{\varphi}\rangle=\langle\widehat{\psi}\mid Q\mid\widehat{\phi}\rangle\widehat{I}\in\widehat{C}_{Q};\ \langle\widehat{\psi}\uparrow\widehat{\psi}\rangle=\widehat{I}. \tag{2.4}$$

Then, operators which are Hermitean (observable) for QM remain Hermitean (observable) for HM, as was first proved in [15].

The liftings of the Hilbert space then require corresponding isotopies of all conventional operations [13,14]. We here mention isounitarity  $\widehat{U}*\widehat{U}^{\dagger}=\widehat{U}^{\dagger}*\widehat{U}=\widehat{I};$  the isoeigenvalue equations  $H*\mid\widehat{\psi}\rangle=+HQ\mid\widehat{\psi}\rangle=\widehat{E}*\mid\widehat{\psi}\rangle\equiv E\mid\widehat{\psi}\rangle;$  the isoexpectation values  $\widehat{A}$  = =  $\langle\widehat{\psi}\mid QAQ\mid\widehat{\psi}\rangle/\langle\widehat{\psi}\mid Q\mid\widehat{\psi}\rangle;$  etc.

The lifting of the unit, base field and carrier space then require, for mathematical consistency, the lifting of the entire structure of Lie's theory, that is, the isotopies of enveloping associative algebras  $\xi$ , Lie algebras L, Lie groups G, representation theory, etc. [7—9]. Here we mention the isoassociative enveloping operator algebras  $\hat{\xi}_Q$  with isoprocuct (2.2);  $A*B \equiv AQB$  the Lie-isotopic algebras  $\hat{L}_Q$  with isoproduct

$$[A, B]_{\hat{\xi}_0} = [A, B] = A * B - B * A \equiv AQB - BQA;$$
 (2.5)

the (connected) Lie-isotopic groups  $\hat{G}_Q$  of isolinear isounitary transforms on  $\hat{E}_Q(z,\overline{z},\hat{\delta},\hat{C})$ 

$$z' = \widehat{U}(w) * z = \widehat{U}(w)Qz = \widehat{U}(w)Q(z, \overline{z}, \dot{z}, \overline{\dot{z}}, \widehat{\psi}, \widehat{\psi}^{\dagger}, ...)z \qquad (2.6a)$$

$$\widehat{U}(w) = e^{iX+\widehat{w}}_{|\widehat{\xi}_{Q}} = \{e^{iXQw}\}\widehat{I}, \qquad (2.6b)$$

$$\widehat{U}(w) * \widehat{U}(w') = \widehat{U}(w') * \widehat{U}(w) = \widehat{U}(W + w'),$$

$$\widehat{U}(w) * \widehat{U}(-w) = \widehat{U}(0) = \widehat{I},$$
(2.6c)

where the reformulation in terms of the conventional exponentiation has been done for simplicity of calculations.

The isounitary  $\hat{U}_{O}(2)$  symmetry is the most general possible, nonlinear, nonlocal and noncanonical, simple, Lie-isotopic invariance group of separation (2.3b) with realization in terms of isounitary operators on

$$\widehat{U} * \widehat{U}^{\dagger} = \widehat{U}^{\dagger} * \widehat{U} = \widehat{I} = Q^{-1}, \tag{2.7}$$

verifying isotopic laws (2.6).

 $\widehat{U}(2)$  can be decomposed into the connected, special isounitary symmetry  $\widehat{SU}_O(?)$  for

 $\det(\widehat{U}Q) = +1,$ (2.8)

plus a discrete part which is similar to that for O(3) [10] and is here ignored for brevity.

The connected  $\widehat{SU}_{O}(2)$  components admit the realization in terms of the generators  $\hat{J}_k$  and parameters  $\theta_k$  of SU(2)

$$\widehat{U} = \prod_{k} e_{\widehat{\xi}}^{i \widehat{J}_{k} + \widehat{\theta}_{k}} = \left\{ \prod_{k} e^{i \widehat{J}_{k} Q \theta_{k}} \right\} \widehat{I}, \qquad (2.9)$$

under the conditions 
$$\operatorname{tr}(\hat{J}_k Q) \equiv 0, \quad k = 1, 2, 3.$$
 (2.10)

The isorepresentations of the isotopic algebras  $\widehat{SU}_{O}(2)$  can be studied by imposing that the isocommutation rules have the same structure constants of SU(2), i.e., for the rules

$$[\widehat{J}_{i},\widehat{J}_{i}] = \widehat{J}_{i}Q\widehat{J}_{i} - \widehat{J}_{i}Q\widehat{J}_{i} = i\varepsilon_{ijk}\widehat{J}_{k}. \tag{2.11}$$

with isocasir1ir

$$\widehat{J}^{\widehat{2}} = \sum_{k} \widehat{J}_{k} * \widehat{J}_{k}, \qquad (2.12)$$

and maximal isocommuting set  $\hat{J}^2$  and  $\hat{J}_3$  as in the conventional case. These assumptions ensure the local isomorphisms  $\hat{SU}(2) \approx SU(2)$  by construction.

Let  $|\hat{b}_k^d\rangle$  be the d-dimensional isobasis of  $\hat{SU}_O(2)$  with iso-orthogonality conditions

$$\langle \hat{b}_i^d \mid * \mid \hat{b}_j^d \rangle := \langle \hat{b}_i^d \mid Q \mid \hat{b}_j^d \rangle = \delta_{ij}, \quad i,j = 1, 2, ..., n. \tag{2.13}$$

By putting as in the conventional case  $\hat{J}_{\pm} = \hat{J}_{1} \pm \hat{J}_{2}$ , and by repeating the same procedure as the familiar one [1], we have

$$\hat{J}_{3} * | \hat{b}_{k}^{d} \rangle = b_{k}^{d} | \hat{b}_{k}^{d} \rangle, \quad \hat{J}^{2} * | \hat{b}_{k}^{d} \rangle = b_{1}^{d} (b_{1}^{d} - 1) | \hat{b}_{1}^{d} \rangle, 
d=1,2,..., k=1,2,...,d, b_{1}^{d} \equiv -b_{d}^{d}, b_{1}^{d} (b_{1}^{d} - 1) \equiv b_{d}^{d} (b_{d}^{d} + 1).$$
(2.14)

A consequence is that the dimensions of the isorepresentations of  $\widehat{SU}_Q(2)$  remain the conventional ones, i.e., they can be characterized by the familiar expression n=2j+1,  $j=0,\frac{1}{2},1,\ldots$  as expected from the isomorphism  $\widehat{SU}_Q(2) \approx SU(2)$ .

However, the explicit forms of the matrix representations are different than the conventional ones, as expressed by the rules

$$(\hat{J}_1)_{ii} = \frac{1}{2}i \mid \hat{b}_i^d \rangle * (\hat{J}_- - \hat{J}_+) * \mid \hat{b}_i^d \rangle,$$
 (2.15a)

$$(\widehat{J}_2)_{ij} = \frac{1}{2} i \mid \widehat{b}_i^d \rangle * (\widehat{J}_- - \widehat{J}_+) * \mid \widehat{b}_j^d \rangle, \qquad (2.15b)$$

$$(\widehat{J}_3)_{ij} = \langle \widehat{b}_i^d \mid * \widehat{J}_3 * \mid \widehat{b}_j^d \rangle, \tag{2.15c}$$

under condition (2.10).

The isorepresentations of the desired dimension can then be constructed accordingly. In the next section we shall compute the two-dimensional isorepresentations, while those of higher dimensions are studied elsewhere [14].

A new image of the conventional SU(2)-symmetry is characterized by our isotopic methods via the antiautomorphic map  $I = \text{diag}(1,1) \Rightarrow I^a = -1$  called *isoduality*, first introduced in [10], which provides a novel and intriguing characterization of antiparticles [14]. The corresponding *isodual*  $\hat{SU}_O^d(2)$  symmetry will be studied in a separate work.

In summary, our isotopic methods permit the identification of four physically relevant isotopies of SU(2) which, for the case of isospin, are given by: the broken conventional SU(2) for the usual treatment of p-n; the exact isotopic  $\widehat{SU}_Q(2)$  for the characterization of p-n (see next section); the broken isodual  $SU^d(2)$  symmetry for the characterization of the antiparticles  $\overline{p}-\overline{n}$  in isodual spaces; and the exact, isodual, isotopic  $\widehat{SU}_Q^d(2)$  for the characterization of antiparticles  $\overline{p}-\overline{n}$  in isodual isospace.

The reader may be interested in knowing that, when the positive- (or negative-) definiteness of the isotopic elemnt Q is relaxed, the isotopes  $\widehat{SU}(2)$  unify all three-dimensional simple Lie groups of Cartan classification over a comples field (of characteristic zero). In fact, we have the compact isotopes  $\widehat{SU}(2) \approx SU(2)$  for  $g_{11} > 0$ ,  $G_{22} > 0$  and the noncompact isotopes  $\widehat{SU}(2) \approx SU(1,1)$  for  $g_{11} > 0$  and  $g_{22} < 0$  (see [10] for the corresponding unification of orthogonal groups over the reals). In this note we consider only positive definite isotopic elements Q.

#### 3. Isotopies of Pauli Matrices

Recall that the conventional Pauli matrices  $\sigma_k$  (see, e.g. [2]) verify the rules  $\sigma_i \sigma_{j, -} = i \, \varepsilon_{ijk} \, \sigma_k$ , i, j, k = 1, 2, 3. In this section we show that the isoalgebra  $SU_q(2)$  implies the existence of intriguing generalizations of these familiar matrices.

To have a guiding principle, we recall that [12], in general, Lie-isotopic algebras are the image of Lie algebras under nonunitary transformations. In fact, under  $\epsilon$  transformation  $UU^{\dagger} \neq I$ , a Lie commutator among generic matrices A, E, acquires the Lie-isotopic form

$$U(AB - BA)U^{\dagger} = A'Q\beta' - B'QA', \tag{3.1a}$$

$$A' = UAU^{\dagger}, \ B' = UBU^{\dagger}, \ Q = (UU^{\dagger})^{-1} = Q^{\dagger}.$$
 (3.1b)

We therefore expect a first class of fundamental (adjoint) isorepresentations characterized by the maps  $J_k = \frac{1}{2} \sigma_k \rightarrow \hat{J}_k = U J_k U^{\dagger}$ ,  $UU^{\dagger} \neq I$ ,  $\pm \frac{1}{2} \rightarrow + \frac{1}{2} f(\Delta)$ ,  $3/4 \rightarrow (3/4) f^2(\Delta)$ , here called regular adjoint isorepresentations of  $\hat{SU}_O(2)$ .

An example is readily constructed via Eqs. (2.15) resulting in the following generalization of Pauli's matrices here called *regular isopauli matrices* 

$$\hat{G}_{1} = \Delta^{-1/2} \begin{pmatrix} 0 & g_{11} \\ g_{22} & 0 \end{pmatrix}, \quad \hat{G}_{2} = \Delta^{-1/2} \begin{pmatrix} 0 & -ig_{11} \\ +ig_{22} & 0 \end{pmatrix},$$

$$\hat{G}_{3} = \Delta^{-1/2} \begin{pmatrix} g_{22} & 0 \\ 0 & -g_{11} \end{pmatrix}, \quad (3.2a)$$

$$[\hat{\sigma}_i, \hat{\sigma}_j] = \hat{\sigma}_i Q \hat{\sigma}_i - \hat{\sigma}_i Q \hat{\sigma}_i = 2i \, \epsilon_{ijk} \hat{\sigma}_k, \ Q = \text{diag}(g_{11}, g_{22}), \quad (3.2b)$$

where  $\Delta = \det Q = g_{11}g_{22} > 0$ , with generalized isoeigenvalues for  $f(\Delta) = \Delta^{1/2}$  and  $\hat{J}_k = \frac{1}{2}\hat{\sigma}_k$ , k = 1, 2, 3,

$$\hat{J}_{3} * | \hat{b}_{i}^{2} \rangle = \pm (1/2) \Delta^{1/2} | \hat{b}_{i}^{2} \rangle,$$
 (3.3a)

$$\hat{J}^{\hat{2}} * | \hat{b}_{i}^{2} \rangle = (3/4)\Delta | \hat{b}_{i}^{2} \rangle, \quad i = 1, 2$$
 (3.3b)

which confirm the «regular» character of the generalization here considered. The isonormalized isobasis is then given by a simple extension of the conventional basis,  $|\hat{b}\rangle = g^{-1/2} |b\rangle$ .

Recall that Pauli's matrices are essentially unique, in the sense that their transformations under unitary equivalence do not yield significant changes in their structure, as well known. The situation is different for the isopauli matrices, because isorepresentations are based on various degrees of freedom which are absent in the conventional SU(2) theory, such as: 1) infinitely possible isotopic elements Q; 2) formulation of the isoalgebra in terms of structure functions [7]; 3) use of an isotopic element for the isohilbert space different than that of the isoalgebra [13,14]; and others.

We shall call irregular adjoint isorepresentations of  $\hat{SU}_Q(2)$  those with generalized eigenvalues other than (3.3), e.g., those of type (1.1). A first example is given by the irregular isopauli matrices

$$\hat{\sigma}_{1} = \begin{pmatrix} 0 & 1 \\ 1 & 0 \end{pmatrix} = \sigma_{1}, \quad \hat{\sigma}_{2} = \begin{pmatrix} 0 - i \\ + i & 0 \end{pmatrix} = \sigma_{2}, 
\hat{\sigma}_{3} = \begin{pmatrix} g_{22} & 0 \\ 0 & -g_{11} \end{pmatrix} = \Delta \hat{I} \sigma_{3}$$
(3.4)

which verify the isocommutation rules with structure functions

$$[\widehat{\sigma}_{1'},\widehat{\sigma}_{2'}] = 2i\,\widehat{\sigma}_{3},\ [\widehat{\sigma}_{2'},\widehat{\sigma}_{3'}] = 2i\,\Delta\,\widehat{\sigma}_{1'},\ [\widehat{\sigma}_{3'},\widehat{\sigma}_{1'}] = 2i\,\Delta\,\widehat{\sigma}_{2'},\ (3.5)$$

without evidently altering the local isomorphisms  $\hat{SU_Q}(2) \approx SU(2)$ .

The new isoeigenvalue equations are given by

$$\hat{J}_{3'} * | \hat{b}_{i}^{2} \rangle = \pm \frac{1}{2} \Delta | \hat{b}_{i}^{2} \rangle, \quad \hat{J}^{2} * | \hat{b}_{i}^{2} \rangle = \frac{1}{2} \Delta (\frac{1}{2} \Delta + 1) | \hat{b}_{i}^{2} \rangle, \quad (3.6)$$

which comfirm the «irregular» character under consideration and provide an illustration of Eqs. (1,1).

Yet anot ier realization of irregular isopauli matrices is given by

$$\widehat{\sigma}_{1}^{\prime\prime} = \begin{pmatrix} 0 & g_{22}^{-1/2} \\ g_{11}^{-1/2} & 0 \end{pmatrix}, \ \widehat{\sigma}_{2}^{\prime\prime} = \begin{pmatrix} 0 & -ig_{22}^{-1/2} \\ ig_{11}^{-1/2} & 0 \end{pmatrix}, \ \widehat{\sigma}_{3}^{\prime\prime} = \begin{pmatrix} g_{11}^{-1} & 0 \\ 0 & g_{22}^{-1} \end{pmatrix},$$
(3.7)

with isocommutation rules and isoeigenvalues

$$[\hat{J}_{1}^{\prime\prime},\hat{J}_{2}^{\prime\prime}] = i\Delta \hat{J}_{3}^{\prime\prime}, \ [\hat{J}_{2}^{\prime\prime},\hat{J}_{3}] = i\hat{J}_{1}^{\prime\prime}, \ [\hat{J}_{3}^{\prime\prime},\hat{J}_{1}^{\prime\prime}] = i\hat{J}_{2}^{\prime\prime},$$
 (3.8a)

$$\widehat{J}_{3}^{'}*|\widehat{b}_{i}^{2}\rangle=\pm\frac{1}{2}|\widehat{b}_{i}^{2},\widehat{J}^{'}\widehat{2}*|\widehat{b}_{i}^{2}\rangle=\frac{1}{2}\left(\frac{1}{2}+\Delta\frac{1}{2}\right)|\widehat{b}_{i}^{2}\rangle. \tag{3.8b}$$

Note that the regular isorepresentations (3.2) are characterized by structure constants; while irregular isorepresentations (3.4) and (3.7) are characterized by structure functions. Intriguingly, the former generally occur in the mathematical study of  $\widehat{SU}_q(2)$ , to have the local isomorphism  $\widehat{SU}_q(2) \approx SU(2)$  by construction, as done in Sect.2. However, the latter generally occur in physical applications [13,14]. This is due to the fact that generators are not changed by isotopies [7–9] (recall that they represent physical quantities). Their embedding in an isotopic algebre then generally implies the appearance of the structure functions.

By no means the above two classes exhaust all possible, physically significant is prepresentations (in fact, we do not study here for brevity the isorepresentations with different isotopic elements for the isoenvelope and isohilbert space). We therefore introduce a third class under the name of standard adjoint isorepresentations, which occur when the eigenvalues are the conventional ones, but the algebra is isotopically nontrivial.

In fact, regular isopauli matrices (3.2) admit the conventional eigenvalue  $\frac{1}{2}$  for  $\Delta = 1$ . This condition can be verified by putting  $g_{11} = g_{22}^{-1} = \lambda$ . We discover in this way the existence of the standard isopauli matrices

$$\widehat{\sigma}_{1} = \begin{pmatrix} 0 & \lambda \\ \lambda^{-1} & 0 \end{pmatrix}, \quad \widehat{\sigma}_{2} = \begin{pmatrix} 0 & -i\lambda \\ i\lambda^{-1} & 0 \end{pmatrix}, \quad \widehat{\sigma}_{3} = \begin{pmatrix} \lambda^{-1} & 0 \\ 0 & -\lambda \end{pmatrix}, \quad (3.9)$$

which admit all conventional eigenvalues and structure constants,

$$|\widehat{J}_{i},\widehat{J}_{i}| = i \,\varepsilon_{iik}\widehat{\sigma}, \quad \widehat{J}_{3} * |\widehat{b}\rangle = \pm \frac{1}{2} |\widehat{b}, \quad \widehat{J}^{2} * |\widehat{b}\rangle = (3/4) |\widehat{b}\rangle \quad (3.10)$$

yet exhibit a «hidden variable»  $\lambda$  in their very structure. Note however that the functional dependence of  $\lambda$  is left completely unrestricted by the isotopy.

Thus,  $\lambda$  can be an arbitrary, real-valued, nowhere null, nonlinear-integral function,  $\lambda = \lambda(z, \varepsilon, \hat{\psi}, \hat{\psi}^{\dagger}, ...) = \bar{\lambda} \neq 0$ .

Needless to say, irregular isorepresentations also become standard under the condition  $\det g = 1$ . We therefore have the following additional standard isopauli matrices

$$\widetilde{\sigma}_{1} = \begin{pmatrix} 0 & 1 \\ 1 & 0 \end{pmatrix} = \sigma_{1}, \quad \widetilde{\sigma}_{2} = \begin{pmatrix} 0 & -i \\ +i & 0 \end{pmatrix} = \sigma_{2}, \quad \widetilde{\sigma}_{3} = \begin{pmatrix} \lambda^{-1} & 0 \\ 0 & -\lambda \end{pmatrix}, \quad (3.11a)$$

$$\widehat{\sigma}_{1}^{"} = \begin{pmatrix} 0 & \lambda^{\frac{1}{2}} \\ \lambda^{-\frac{1}{2}} & 0 \end{pmatrix}, \quad \widehat{\sigma}_{2}^{"} = \begin{pmatrix} 0 & -i\lambda^{\frac{1}{2}} \\ i\lambda^{-\frac{1}{2}} & 0 \end{pmatrix}, \quad \widehat{\sigma}_{3}^{"} = \begin{pmatrix} \lambda^{-1} & 0 \\ 0 & -\lambda \end{pmatrix}$$
(3.11b)

Isopauli matrices with generalized eigenvalues are useful for interior structural problems, i.e., the description of a neutron in the core of a neutron star or, along the same lines, for a hadron constituent. As such, the applications of the general case of the  $\hat{SU}_Q(2)$  isosymmetry is studied elsewhere 1181.

When studying conventional particles, e.g., those of nuclear physics, the subclass of  $\hat{SU}_Q(2)$  which is physically relevant is the special one with conventional eigenvalues which is studied in the next sections. The image  $\hat{\sigma}_k^d$  of (3.9) under isoduality, called *isodual Pauli matrices*, will be studied elsewhere.

### 4. Applications to Isospin in Nuclear Physics

As well known [2], the conventional SU(2)-isospin symmetry is broken by electromagnetic and weak interactions. One of the first applications of our isotopic/Q-operator deformation of SU(2) is to show that the isospin symmetry can be reconstructed as exact at the isotopic level, namely, there exist a realization of the underlying isospace  $\widehat{E}_Q(z, \overline{z}, \widehat{\delta}, \widehat{C})$  in which protons and neutrons have the same mass, although the conventional  $v_i$  lues of mass are recovered under isoexpectation values.

The main idea is that the SU(2)-isospin symmetry is broken when realized in its simplest conceivable form, that via the Lie product AB-BA. However, when the same symmetry is realized via a lesser trivial product, such as our Lie-isotopic product AQB-BQA [7], it can be proved to be exact even under electromagnetic and weak interactions. Actually, the constant Q-matrix acquires the meaning of a suitable average of these interactions.

The reader should be aware that, by no means, this is an isolated occurrence, because it represents rather general capabilities of the Lie-isotopic theory referred to as the isotopic reconstruction of exact space-time and internal symmetries when conventionally broken. For example, the rotational symmetry has been reconstructed as exact for all infinitely possible ellipsoidical deformations of the sphere [10]; the Lorentz symmetry has been reconstructed as exact at the isotopic level for all possible signature preserving deformations  $\hat{\eta} = Q\eta$  of the Minkowski metric [11]; etc.

The reconstruction of the exact  $\hat{SU}_{O}(2)$ -isospin symmetry is so simple to appear trivial. Consider a twelve-component isostate

$$\widehat{\psi}(x) = \begin{pmatrix} \widehat{\psi}_p(z) \\ \widehat{\psi}_n(x) \end{pmatrix}, \tag{4.1}$$

where  $\hat{\psi}_p(x)$  and  $\hat{\psi}_n(x)$  are solutions of the isodirac equation of note [6] which transfroms isocovariantly under  $o(3.1) \times \hat{SU}_{O'}(2)$  for the particular subclass with conventional eigenvalues. In this note we study only the  $\hat{SU}_{O}(2)$  part without any isominkowskian coordinates, thus restricting our attention to the isonormalized isostates

$$|\widehat{\psi}_{p}\rangle = \begin{pmatrix} \lambda^{-\frac{1}{2}} \\ 0 \end{pmatrix}, |\widehat{\psi}_{n}\rangle = \begin{pmatrix} 0 \\ \lambda^{\frac{1}{2}} \end{pmatrix}, \langle \widehat{\psi}_{k} | Q | \widehat{\psi}_{k}\rangle = 1, k = p, n, \tag{4.2}$$

where  $Q \doteq \text{diag.}(\lambda, \lambda^{-1})$ ,  $\widehat{I} = Q^{-1} = \text{diag.}(\lambda^{-1}, \lambda)$ . We then introduce the  $\widehat{SU}_Q(2)$ -isospin with realization (3.9) admitting conventional eigenvalues  $\pm \frac{1}{2}$  and 3/4, defined over the isospace  $\hat{E}_{Q}(z, \overline{z}, \hat{\delta}, \hat{C}), \hat{\delta} = Q\delta.$ 

We now select such isospace to admit the same masses for the proton and the neutron. This is readily permitted by the «hidden variable»  $\lambda$  when selected in such a way that  $m_n \lambda^{-1} = m_n \lambda$ , i.e.,  $\lambda^2 = m_p / m_n = 0.99862$ .

$$m_p \lambda^{-1} = m_n \lambda$$
, i.e.,  $\lambda^2 = m_p / m_n = 0.99862$ . (4.3)

The mass operator is then defined by

$$\hat{M} = \{ \frac{1}{2} \lambda (m_p + m_n) \hat{I} + \frac{1}{2} \lambda^{-1} (m_p - m_n) \hat{\sigma}_3 \} \hat{I} = \begin{pmatrix} m_p \lambda^{-1} & 0 \\ 0 & m_n \lambda \end{pmatrix}$$
(4.4)

and manifestly represents equal masses  $\hat{m} = m_n \lambda^{-1} = m_n \lambda$  in isospace.

The recovering of conventional masses in our physical space is readily achieved via the isoeigenvalue expression on an arbitrary isostate

$$\widehat{M} * |\widehat{\psi}\rangle = \widehat{MIQ} |\widehat{\psi}\rangle = M|\widehat{\psi}\rangle = \begin{pmatrix} m_p & 0 \\ 0 & m_n \end{pmatrix} |\widehat{\psi}\rangle, \tag{4.5}$$

or, equivalently, via the isoexpectation values

$$\langle \widehat{\psi}_{p} | Q \widehat{M} Q | \widehat{\psi}_{p} \rangle = m_{p}, \quad \langle \widehat{\psi}_{n} | Q \widehat{M} Q | \widehat{\psi}_{n} \rangle = m_{n}. \tag{4.6}$$

Similarly, the charge operator can be defined by

$$q = \frac{1}{2} \operatorname{e} (\widehat{I} + \widehat{\sigma}_3) = \begin{pmatrix} \operatorname{e}\lambda^{-1} & 0 \\ 0 & 0 \end{pmatrix}. \tag{4.7}$$

Thus, the  $\hat{SU}_Q(2)$  charges on isospace are  $q_p = e\lambda^{-1}$  and  $q_n = 0$ . However, the charges in our physical space are the conventional ones,

$$\langle \hat{\psi}_{p} | QqQ | \hat{\psi}_{p} \rangle = e, \ \langle \hat{\psi}_{n} | QqQ | \hat{\psi}_{n} \rangle = 0.$$
 (4.8)

The isodual  $\hat{SU}_Q^d(2)$ -isospin characterizes the antiparticle  $\bar{p}$  and  $\bar{n}$  will be studied elsewhere.

The entire theory of isospin and its applications [2] can then be lifted in an isotopic form which remains exact under all interactions [14]. This is not a mere mathematical curiosity, because it implies a necessary isotopy of the nuclear force, e.g., via  $\hat{SU}_O(2)$ -isotopic exchange mechanism.

These dynamical implications are studied elsewhere. We orly mention that their physical origin lies in the old hypothesis that nuclear forces have a (very small) nonlocal-nonhamiltonian component due to the overlapping of the charge distributions of nucleons. The \*hidden variable\*  $\lambda$  here introduced merely provides an average of these novel components of the nuclear force.

### 5. Application to Few-Body Nuclear Magnetic Moments

In the recent note [6] we have shown that the  $\hat{SU}_Q(2)$  symmetry permits a direct representation of: 1) the expected nonspherical shapes of the charge distribution of nucleons; 2) all their infinitely possible deformations due to external forces; and 3) the consequential alteration of the «intrinsic» magnetic moment of protons and neutrons under sufficient conditions.

These results were then applied in note [6] to the apparently first, exact representation of the total magnetic moment of the deuteron and other few-body nuclei.

It is now recommendable to re-examine these results within the context of the exact isospin symmetry of this note.

Consider nuclei with A even and introduce (A/2)-dimensional isospaces  $\hat{E}_k(z,\hat{\delta},\hat{C}), \hat{\beta} = Q_k \delta$ , isotopic elements  $Q_k = \text{diag.}(\lambda_k,\lambda_k^{-1}), \det Q_k = 1$ , isounits  $\hat{I}_k = Q_k^{-1}$ , and related  $\hat{SU}(2)$  isosymmetry for isospin  $\frac{1}{2}$  (the extension to odd A is the same as in QM). As well known (see, e.g., [2,3]), total nuclear magnetic moments are computed via the familiar expressions

$$\mu^{(S)} = g^{(s)} (eh/2m_p c_0) S, \quad g_p^{(s)} = 5.585,$$

$$g_n^{(s)} = -3.816, \quad eh/2m_p c_0 = 1,$$
(5.1a)

$$\mu^{(L)} = g^{(L)}L, \ g_p^{(L)} = 1, \ g_n^{(L)} = 0.$$
 (5.1b)

In the p ecceding section we selected the whidden parameter»  $\lambda$  to identify the p and n masses. We here select the  $\lambda$ -parameter to render equal the (magnitude of the) p-n magnetic moments via the model

$$\hat{\mu} = \{ \frac{1}{2} \lambda (g_p + g_n) \hat{I} + \frac{1}{2} \lambda^{-1} (g_p - g_n) \hat{\sigma}_3 \} \hat{I} = \text{diag.} (g_p \lambda^{-1}, g_n \lambda), \quad (5.2a)$$

$$\widetilde{g} = \lambda^{-1} g_{p}^{(S)} = -\lambda g_{n}^{(S)}, \ \langle \widehat{\psi}_{k} | Q \mu Q | \widehat{\psi}_{k} \rangle = g_{k}, \ k = p, n. \tag{5.2b}$$

A simple isotopic lifting of the conventional QM isospin treatment (see [14] for details), then leads to the following alternative formulation of model (3.9) of note [6]

$$\widehat{\mu}_{\text{Tot}}^{HM} = \frac{1}{2} \sum_{k} \widehat{I}_{k} \times L_{k3} + \sum_{k} (\frac{1}{2} L_{k3} + \widetilde{g}_{k} \tau_{k3} \times S_{k3}).$$
 (5.3)

Recall that, in the conventional treatment we have two terms, called scalar and vector components, with the latter being dominant over the former. The dominance of the latter becomes greater under isotopies, and constitutes the sole contribution for L=0.

Consider now the case of the Deuteron (D) and the experimental value of its magnetic moment

$$\mu_0^{\text{exp}} = 0.857, \ (\mu_p = 1).$$
 (5.4)

As well known, in OM we have the theoretical value

$$\mu_D^{QM} = g_p + g_n = 0.879, \tag{5.5}$$

which, as such, does not represent value (5.4) exactly, while significant differences persist under relativistic, L=2 and other corrections (L=1 is prohibited by parity [2,3], while many-body techniques are evidently inapplicable for the deuteron).

In note [6] we provided the exact representation of value (5.4) via a mutation  $\hat{\mu}_p$ ,  $\hat{\mu}_n$  of the p-n magnetic moments due to a small deformation of their charge distributions. In this note we present the same result, but this time obtained in an isospace with exact isospin symmetry and equal magnitudes of the p-n magnetic moments in the deuteron, which is achieved for value, in  $\hat{E}(r, \bar{r}, \delta, \hat{C})$ 

$$\lambda^2 = |g_n|/|g_n| = 3.816/5.5816 = 0.685, \ \widetilde{g} = 0.428.$$
 (5.6)

The use of the HM formalism then yields the isoeigenvalues of (5.3)

$$\hat{\mu}_D^{HM} * \hat{\psi} = 2\hat{g}\tau_3 \times S_3 Q \hat{\psi} + 2\tilde{g}\hat{\psi} = 0.857 \hat{\psi}. \tag{5.7}$$

This illustrates the possibility of exactly representing  $\mu_D^{\rm exp}$  as already done in Sect. 3B of [6], but under the additional condition of having the same magnitude of the p-n magnetic moments in isospace.

### Acknowledgments

The author would like to express his appreciation to the JINR for kind hospitality, and for its unique atmosphere of free pursue of novel physical knowledge.

#### References

- 1. Edmonds A.R. Angular Momentum in Quantum Mechanics, Princeton Univ. Press, 1960.
  - Brink D.M., Satchler G.R. Angular Momentum, Clarendon Press Oxford, England, 1968.
- 2. Eder G. Nuclear Forces, MIT press, 1968.
- Blatt J.M., Weiskopf V.F. Theoretical Nuclear Physics, Wiley, New York, 1964.

- 4. Curtright T.L., Fairlie D.B., Zachos Z.K., Editors. Quantum Groups, World Scientific, 1991.
  - Smirno / Yu.F., Asherova R.M., Editors. In: Proceedings of the Fifth Workshop Symmetry Methods in Physics, JINR, Dubna, 1992.
- 5. Lopez I).F. Origin and Axiomatization of q-Deformation. In: Proceedings of the International Workshop on Symmetry Methods in Physics, JINR, Dubna, 1993.
- Santilli R.M. A Quantitative Isotopic Representation of the Deuteron Magnetic Moment. In: Proceeding of Deuteron 1993, JINR Dubna, 1993.
- Santilli R.M. Hadronic J., 1978, 1, p.228, p.1279; Phys. Rev., 1979, D20, p.55; Foundations of Theoretical Mechanics, vol.II, Springer-Verlag, 1983.
- 8. Kadeisvill J.V. In: Proceedings of the International Workshop on Symmetry Methods in Physics, JINR, Dubna, 1993.
- 9. Sourlas D.S., Tsagas G.T. Mathematical Foundations of the Lie-Santilli Theory, Ukraine Academy of Sciences, to appear, 1993.
- 10. Santilli R.M. Hadronic J., 1985, 8, p.25, p.36.
- 11. Santilli R.M. Lett. Nuovo Cimento, 1983, 37, p.545; 1983, 38, p.509.
- 12. Santilli R.M. Hadronic J., 1978, 1, p.578.
- 13. Santilli R.M. Hadronic J., 1992, 15, p.1.
- 14. Santilli R.M. Elements of Hadronic Mechanics, vols.I, II, III, to appear, 1994.
- Myung H., Santilli R.M. Hadronic J., 1982, 5, p.1277, p.1367.
   Mignani R., Myung H.C., Santilli R.M. Hadronic J., 1983, 6, p.1878.
- 16. Santilli R.M. Algebras, Groups and Geometries, 1993, 10, p.373.
- 17. Kadeisvili J.V., Kamiya M., Santilli R.M. Hadronic J., 1993, 16, p.168.
- Santilli R.M. Isotopies of Quark Theories. In: Proceedings of the XVI Workshop on High Energy Physics and Field Theory, IHEP, Protvino, 1993.
- 19. Bohm D. Quantum Theory, Dover Publ., 1989.
- 20. Santilli R.M. In: Proceedings of the International Conference on Frontiers of Fundamental Physics, Plenum Publ., 1993.

#### SOLUTION TO THE ONE-DIMENSIONAL CLUSTER MODEL

#### A.V.Bakaev\*, V.I.Kabanovich\*

A one-dimensional lattice gas model is considered, in which in eract only particles inside a cluster. Exact recursion relations for the partition function are obtained and solved in the thermodynamic limit. The c uster size distribution function is determined. Conditions for a thermodynamic size cluster to coexist with vapor are found.

The investigation has been performed at the Bogoliubov Laboratory of Theoretical Physics, JINR.

#### Решение одномерной кластерной модели

#### А.В.Бакаев, В.И.Кабанович

Рассмотрена одномерная модель решеточного газа, в которой вззимодействуют только частицы внутри одного кластера. Получены точные рекурсивные соотношения для статистической суммы, которые решены в термодинамическом пределе. Определена функция распределения ; азмеров кластера. Найдены условия, при которых кластер термодинамического размера сосуществует с паром.

Работа выполнена в Лаборатории теоретической физики им. Н Н.Боголюбова ОИЯИ.

Let  $\mathcal{L}$  be a 1D lattice (ring) of V sites each of which either is vacant or contains a particle. The total number of particles is equal to N. By a cluster  $\mathcal{C}_k$  we mean a set of k particles on  $\mathcal{L}$  which constitute a chain of nearest neighbour on  $\mathcal{L}$ . Let the energy of an arbitrary particle configuration be given by

 $\mathcal{H} = \sum_{k} \varepsilon(k) \, n(k), \tag{1}$ 

where  $\varepsilon(k)$  is the energy of a  $C_k$ , and n(k) is the number of such clusters. This model belongs to the class of Polymer Models (see [1]) the one in which we fix only the total number of particles and not the numbers of clusters of each type. The examples of such models include, in particular, the nearest-neighbour interaction 1D lattice gas, and the 1D

e-mail: AVB@SMS.CCAS.MSK.SU

<sup>\*</sup>Computing Centre of the Russian Academy of Sciences, 40 Vavilov Str., GSP-1, 117333, Moscow, Russia

version of a hole-induced frustration spin model, in which the spin variables can be summed out leading to an effective hole Hamiltonian of the form (1) (see [2]).

It is well known that lattice gas type models rapidly decaying pair interactions cannot have long-range order at non-zero temperatures; the models with the potential  $\propto 1/x^2$  exhibit a first order transition in temperature (see [3], and [4], [5]), and for stronger interactions, for instance for the Coulomb potential [6], which is  $\propto x$  in one dimension, classical particles condense, or crystallize, at all temperatures. The simple cluster model (1) considered in this paper seems to have to do with both the cases. In particular, for some cluster energies condensation arises even in one dimension.

The partition function of the system with the interaction (1), laid on the 1D lattice  $\mathcal{L}$  with free boundary conditions, is given by

$$Z_{f}(V, N) = \sum_{\{n(k)\}} C(V, N, \{n(k)\}) \delta\left(N - \sum_{k=1}^{\infty} kn(k)\right) \exp(-\beta \mathcal{H}), \quad (2)$$

where  $C(V, N, \{n(k)\})$  is the number of particle configurations which form a given set  $\{n(k)\}$  of the numbers of clusters:

$$C(V, N, \{n(k)\}) = \frac{(V - N + 1)!}{\sum_{k=0}^{\infty} n(k)!}, \quad n(0) = V - N + 1 - \sum_{k=1}^{\infty} n(k).$$
(3)

Let us mention that the partition function of the noninteracting Boltzmann gas of  $N_B = V - N + 1$  particles with the discreet spectrum  $\varepsilon_B(k) = \varepsilon(k), \ k = 1, ..., \varepsilon_B(0) = 0$ , differs from (2) only by the  $\delta$ -factor

 $\delta (N - \sum_{k=1}^{\infty} kn(k))$  which can be considered as some artificial non-ideality of the Boltzmann gas.

Summing the contributions due to configurations in which the first site of the chain belongs to  $C_k$ , k=1,...,N, or is empty (k=0), we obtain the following recurrence:

$$Z_{f}(V, N) = \sum_{k=0}^{N} v(k) Z_{f}(V - k - 1, N - k), V > N \ge 0,$$

$$Z_{f}(V, V) = 1, V \ge 0.$$
(4)

where  $v(k) = \exp(-\beta \varepsilon(k))$ , k = 1, 2, ..., N, and we put, formally, v(0) = 1.

For  $\mathcal{L}$  with periodic boundary conditions we have:

$$Z_{p}(V,N) = \sum_{k=0}^{N} (k+1) v(k) Z_{f}(V-k-2,N-k), \quad V \ge N+2.$$
 (5)

Let c(k) be the average number of clusters  $C_k$ ,  $c(k) = \langle n(k) \rangle$ . It is not hard to prove that

$$c(k) = Vv(k) \frac{Z_{f}(V - k - 2, N - k)}{Z_{p}(V, N)}, \qquad k = 1, ..., N.$$
 (6)

Using the normalization condition  $N = \sum_{k=1}^{N} kc(k)$ , we get

$$\frac{\sum_{k=0}^{N} k v(k) Z_{f}(V-k-2, N-k)}{N} = \frac{N}{V} \equiv \rho.$$

$$\sum_{k=0}^{N} (k+1) v(k) Z_{f}(V-k-2, N-k)$$
(7)

Since Eq. (7) holds for any (V, N), for the sequence  $S(j) = Z_f(V - N - 2 + j, j)$ , j = 0,..., N, where V and N are fixed, from Eq. (7) we get the following recurrence:

$$S(j) = \sum_{k=1}^{j} \left( (V - N) \frac{k}{j} - 1 \right) v(k) S(j - k), \quad S(0) = 1.$$
 (8)

Thus, to compute  $Z_p(V,N)$  and c(k), k=1,2,...,N, it will suffice to use the recurrence (8) only N times, instead of applying Eq. (4) more than  $N^2/2$  times.

Suppose that the limit  $v = \lim_{k \to \infty} (v(k))^{1/k}$  exists. For any positive r, the quantities c(k) are invariant with respect to the transformation

$$v(k) \to v'(k) = v(k)r^k, \quad Z_f(V, N) \to Z_f(V, N) = Z_f(V, N).$$
 (9)

Thus, choosing  $r = v^{-1}$  we reduce the model to the case v = 1.

Let us start from the case in which only a number of the first terms contribute to the sums in Eq. (7). Then, for sufficiently large (V, N), we have

$$\frac{Z_f(V-k-2,N-k)}{Z_f(V-2,N)} \simeq \exp(k\beta(\mu-p)) \equiv \alpha^k, \tag{10}$$

where p and  $\mu$  are the pressure and chemical potential in the limit  $V \to \infty$ ,  $N_i V = \rho$ , respectively. If  $\alpha < 1/v = 1$ , then the contributions to the sums in Eq. (7) decrease exponentially, and in the thermodynamic limit the density  $\rho$  as a function of the parameter  $\alpha$  is given by

$$\rho = \frac{\sum_{k=0}^{\infty} kv(k) \alpha^{k}}{\sum_{k=0}^{\infty} (k+1) v(k) \alpha^{k}},$$
(11)

and the average numbers of clusters decrease exponentially,

$$c(j) = \frac{Vv(j) \alpha^{j}}{\sum_{k=0}^{\infty} (k+1) v(k) \alpha^{k}}.$$
 (12)

Denoting  $N_R = V - N$ , we can rewrite (12) in the form:

$$\frac{c(j)}{N_B} = \frac{v(j) \alpha^j}{\sum_{k=0}^{\infty} v(k) \alpha^k},$$
(13)

which gives exactly the occupation numbers of the noninteracting Boltzmann gas with the chemical potential  $\mu_R=\ln\alpha$ .

The function  $\rho(\dot{\alpha})$  (11) is a monotone increasing function of  $\alpha$ , and

$$\rho(0) = 0$$
. It the series  $\sum_{k=0}^{\infty} kv(k)$  diverges, then  $\rho(1) = 1$  and for any

 $\rho \in (0, 1)$  Eq. (11) is the equation of state for the cluster model. If, conversely, this series converges, then  $\rho_c \equiv \rho(1) < 1$ , and at  $\rho > \rho_c$  Eq. (11) has no solution. Thus we have obtained the condition under which the delta-factor in (2) makes this model essentially different from the non-interacting Boltzmann gas.

Numerical calculations by the recurrence (8) in the case  $\rho_c < 1$  demonstrate that S(j) has a maximum at  $j = N_g \propto \kappa(\rho_c)$  (V - N), which gets sharper with the increase of (V - N) (the coefficient  $\kappa(\rho_c)$  is independent of (V, N).

In order to obtain the asymptotical solution to the model with  $\rho > \rho_c$ , we approximate S(j) in the vicinity of its maximum by the following expression:

$$S(N_g + l) = S(N_g) \exp\left(-\frac{l^2}{2D}\right), \quad l << N_g.$$
 (14)

The quantity

$$\Delta(l) = \sum_{k=0}^{N_g} \left( (V - N) \frac{k}{N_g + l} - 1 \right) v(k) \exp\left(-\frac{(l - k)^2}{2D}\right)$$
 (15)

is the difference between the l.h.s. and r.h.s. of Eq. (8) at  $j=N_g+l$ , neglecting the contributions due to k close to  $N_g$ . Choosing the optimal values of  $N_g$  and D from the conditions  $\Delta(0)=0$  and  $\Delta'(0)=0$  we are led to the equations:

$$N_g = (V - N) \frac{\sigma_1}{\sigma_0}; \qquad D = (V - N) \frac{\sigma_2 \sigma_0 - (\sigma_1)^2}{(\sigma_0)^2},$$

$$\sigma_v = \sigma_v (N_g, D) = \sum_{k=0}^{N_g} k^{\nu} v(k) \exp\left(-\frac{k^2}{2D}\right). \tag{16}$$

If  $\rho_c < \rho \le 1$ , then, using Eq. (11) at  $\alpha = 1$  to find the limit of the quantity  $\sigma_1/\sigma_0$ , we get the asymptotics of the solution to Eq. (16):

$$\rho_{g} \equiv \lim_{V \to \infty} \frac{N_{g}}{V} = \rho_{c} \frac{1 - \rho}{1 - \rho_{c}}, \qquad \lim_{V \to \infty} \frac{\sqrt{D}}{V} = 0.$$
 (17)

The function (14) is the asymptotically exact solution to Eq. (8) for |l| < L(V), where L(V) is a function of order of magnitude o(V). Now, using (14), we find the asymptotically exact solution to Eq. (8):

$$S(\rho'V) \sim \sqrt{2\pi D}S(N_g) (V - N) \frac{v(\rho'V - N_g)}{\sum_{k=0}^{\infty} v(k)}, \quad \rho' \in (\rho_c, \rho)$$
 (18)

(we assume, for simplicity, that v(k) is sufficiently smooth at large k). Let  $\rho_{v}(j)$  be the partial densities. According to (6),

$$\rho_{V}(j) = \frac{jc(j)}{V} = \frac{jv(j) S(N-j)}{N} .$$

$$\sum_{k=0}^{N} (k+1) v(k) S(N-k)$$
(19)

Substituting (14), (17), and (18) into (19), we get the following asymptotics for small clusters and macro-clusters, respectively:

$$\rho_V(j) \sim \frac{N_g}{V} \frac{jv(j)}{\infty}, \qquad j << N - N_g,$$

$$\sum_{k=0}^{\infty} kv(k)$$
(20)

$$\rho_V(N - N_g + l) \sim \frac{N - N_g}{V} \frac{1}{\sqrt{2\pi D}} \exp\left(-\frac{l^2}{2D}\right), \quad l << N - N_g.$$
(21)

Clearly, the total density for small clusters is equal to  $\rho_g$  (17), that is  $N_g$  and  $N-N_g$  are the average numbers of particles in the vapor and in the condensate, respectively. The quantity  $\sqrt{D}$  describes the fluctuations of these quantities. Taking the sum of c(k) over macro-clusters  $k\approx N-N_g$  we see that the condensate consists of exactly one macro-cluster. The density of the vapor in its volume  $V-N+N_g$  equals  $\rho_c$ , that is for  $\rho \geq \rho_c$  the vapor is always a critical gas and all extra-particles are condensed into the macro-cluster.

As an example, let us consider the model  $\varepsilon(k) = \ln(k+1)$ . At high temperatures  $0 < \beta < \beta_c = 2$  the system is gaseous at any density. At low temperatures  $\beta > \beta_c$  the system is gaseous if  $\rho < \rho_c(\beta)$ , where

$$\rho_c(\beta) = 1 - \frac{\zeta(\beta)}{\zeta(\beta - 1)}, \qquad \zeta(\beta) = \sum_{k=1}^{\infty} k^{-\beta}, \qquad (22)$$

and at  $\rho > \rho_c$  an equilibrium coexistence of critical vapor and condensate occurs.

#### References

- 1. Gruber C., Kunz H. Comm. Math. Phys., 1971, 22, p.133.
- Bakaev A.V., Ermilov A.N. One Dimensional Spin Model of Phase Separation, Phys. Lett. A, 1993, accepted.
- 3. Thouless P.J. Phys. Rev., 1969, 187, p.732.
- 4. Frohlich J., Spencer T. Commun. Math. Phys., 1982, 84, p.87.
- 5. Aizenman M., Chayes J.T., Chayes L., Newman C.M. J. Stat. Phys., 1988, 50, p.1.
- Choquard Ph., Kunz H., Martin Ph.A., Navet M. One-Dimensional Coulomb Systems, in: Physics in One Dimension, eds. J.Bernasconi and T.Schneider, Springer, Berlin, 1981.

Received on November 11, 1993.

# ACCELERATION OF DEUTERONS AT THE UNK (Proposal)

A.A.Vasil'ev<sup>1</sup>, S.B.Vorozhtsov, V.P.Dmitrievsky, E.A.Myae<sup>2</sup>, V.A.Teplyakov<sup>2</sup>

In this article possible perspectives of using UNK for accelerating multicharged iones with minimal additions and changings in systems of complex UNK are considered. Deuteron accelerating is proposed as the minimum variant in which one supposes to reach energy till 1.5 TeV/nuc in one beam.

The investigation has been performed at the Laboratory of Nuclear Problems, JINR.

#### Ускорение дейтронов в УНК (Предложение)

#### А.А.Васильев и др.

В данной работе рассмотрены перспективы возможного использования УНК для ускорения многозарядных ионов с минимальными изменєниями и дополнениями в системах комплекса. В качестве минимального в грианта в этом плане рассматривается дейтронный режим, в котором предполагается достигнуть энергии вплоть до 1,5 ТэВ/нуклон в одном пучкс.

Работа выполнена в Лаборатории ядерных проблем ОИЯИ.

#### 1. Introduction

The acceleration-and-storage complex (UNK) to be built in the Institute of High Energy Physics (IHEP) is designed for acceleration of intense proton beams (up to  $5 \cdot 10^{14}$  particles/pulse) in the synchrotron mode [1] and for investigations with secondary beams from the fixed target or with colliding proton-proton beams of energy up to 3 TeV. Totally, the complex consists of a 30 MeV linear accelerator with rad o-frequency quadrupole focusing [2], a 1.5 GeV fast-cycling booster synchrotron (25 Hz) [3], a 70 GeV strong focusing synchrotron and three synchrotrons of the UNK proper with the orbit perimeter 20777.8 m and energy 400 GeV (600 GeV in the accelerating mode) and 2x3 TeV. The last two accelerators involve a magnet structure with superconducting elements. The first stages

<sup>&</sup>lt;sup>1</sup>Atomic Power Ministry of the Russian Federation, Moscow.

<sup>&</sup>lt;sup>2</sup>Institute of High Energy Physics, Protvino, Russia.

envisage construction of a 600 GeV accelerator and later one of the 3 TeV rings.

The present work deals with the possible use of the UNK for acceleration of multicharged ions with minimum modification of the UNK systems. Acceleration of multicharged ions was carried out at many high energy accelerators for investigations in the field of relativistic nuclear physics. For example, 9 GeV/c deuterium nuclei were accelerated for the first time at the JINR synchrophasotron in 1970 [4]. Later helium nuclei were accelerated there as well. In the 1970s, deuterons and  $\alpha$ -particles were also accelerated at CERN, where they used the ISR facility designed for colliding proton-proton beams. In 1986-87, <sup>16</sup>O and <sup>32</sup>S with energy 200 GeV/nucleon were obtained there at the SPS. Similar research was carried out at the proton synchrotron AGS in Brookhaven (USA) (16O of energy 15 GeV/nuclein and <sup>28</sup>Si of energy 14.6 GeV/nucleon). At present the growing interest in studying a new state of nuclear matter, which is quark-gluon plasma, results in construction of facilities for acceleration of heavy ions to ultrarelativistic energies. We mean the collider RHIC in Brookhaven, where experimenters will be able to work with particles from protons of energy 250 GeV and luminosity  $\approx 10^{31}$  cm<sup>-2</sup>s<sup>-1</sup> to Au of energy 100 GeV/nucleon and luminosity  $\approx 2 \cdot 10^{26} \, \text{cm}^{-2} \text{s}^{-1}$ . Besides, the large hadron col ider (LHC) at CERN is known to allow not only proton-proton and proton-electron beams but also colliding <sup>208</sup>Pb — <sup>208</sup>Pb beams of centre-of-mass energy 1312 TeV and luminosity  $\approx 1 \cdot 10^{28} \text{ cm}^{-2} \text{s}^{-1}$ .

From the aforesaid, it is clear why there arises interest in extending the capabilities and modification of the UNK, in construction of which large material resources are invested. As a maximum, we consider deuteron acceleration where energy up to 1.5 TeV/nucleon in a beam is supposed to be attained. Of great interest is also an investigation into a possibility of accelerating a beam of polarised deuterons. In ref. [5] the authors already touched upon the problem of conserving proton beam polarisation in the booster synchrotron U-1.5 and in the proton synchrotron U-70. However, for a deuteron beam the expected depolarisation effects seem to be less essential than for a proton beam.

## 2. General Physical Premises for Transition to the Deuteron Range

Since all the accelerators of the complex (except the injector linac) are alternating gradients synchrotrons, transition to the deuteron range is determined by physical features of operation of this type of accelerator.

The main parameters of alternating-gradient synchrotrons are:

- 2.1. acceleration energy range,
- 2.2. acceleration frequency range,
- 2.3. dynamic characteristics and transition energy,
- 2.4. maximum charge density in a bunch,
- 2.5. maximum vacuum in a chamber,
- 2.6. luminosity.

It implies preserving the magnetic structure of the rings and the maximum induction of the magnetic field.

2.1. Acceleration energy range. The total energy of a particle is

$$E = \sqrt{[P^2c^2 + E_0^2]},\tag{1}$$

where  $E_0$  is the rest energy, P is the momentum of the charged particle,

$$P = \frac{eBk_f L_{c0}}{2\pi},\tag{2}$$

 $L_{e0}$  is the length of a closed orbit,  $k_f = \frac{R}{\rho}$  is the factor of filling the orbit with

dipoles,  $R = \frac{L_{e0}}{2\pi}$ ,  $\rho$  is the orbit curvature radius in dipoles, B is induction of the magnetic field in dipoles.

In the relativistic case  $(E >> E_0)$  we have

$$E \approx Pc.$$
 (3)

It directly follows from (2) and (3) that the maximum total energy of an accelerated particle in the given structure of the magnetic field  $(B_{\max}k_fL_{e0}=\text{const})$  is proportional to the charge of a particle undergoing acceleration (e), i.e., the proton ring corresponding to the energy 3 TeV will also hold 3 TeV deuterons.

2.2. Acceleration frequency range. Since the revolution frequency on a closed orbits is

$$f = \frac{\beta c}{L_{e0}},\tag{4}$$

the frequency range is only determined by the velocity of an ion  $(\beta c)$  at injection and at final energy.

In a non-relativistic case  $(\gamma = \frac{E}{E_0} \approx 1)$ 

$$f \approx \sqrt{\frac{W}{m}},$$
 (5)

where W is the kinetic energy and m is the mass of a particle. Here and on the symbol « » indicates that under the given conditions the proportionality constants are the same for protons and deuterons.

At the relativistic energy  $(\gamma >> 1)$ 

$$f \sim 1 - \frac{1}{2v^2}.$$
(6)

In this case the frequency band width is

$$\delta f = \frac{\gamma_k^2 - \gamma_i^2}{2\gamma_k^2 \gamma_i^2} \frac{c}{L_{e0}},$$
 (7)

where  $\gamma_k$ ,  $\gamma_i$  correspond to the final energy and injection energy.

2.3. Dynamic characteristics and transition energy. Within the single-particle theory (without allowance for space charge) betatron frequencies only depend on the magnetic field structure and do not depend on the charge and mass of the particle undergoing acceleration in the synchrotron mode.

The difference occurs in the transition energy, which, at the given expansion coefficient of closed orbits  $\alpha = \frac{P}{L_{e0}} \frac{\delta L_{e0}}{\delta P}$ , is found from

$$E_{tr} = \frac{E_0}{\sqrt{\alpha}},\tag{8}$$

i.e., for the given magnetic structure the kinetic energy increases by a factor of A as compared with protons, where A is the number of nucleons of the given ion. There are several methods of overcoming or elimination of transition energy [6,7,8]. It should be considered in each particular case, which of them is the best.

2.4. Maximum charge density in a bunch. The maximum charge density in its transverse effect at the fixed length of the closed orbit  $L_{e0}$  and the frequency of free oscillations  $(Q_z, Q_p)$  is

$$k \sim \frac{E_0 \gamma^3 \beta^2}{e^2} \sim \frac{EP^2}{E_0^2},$$
 (9)

where the values of  $\gamma$ ,  $\beta$ , P correspond to the energy of injection in the ring,

$$P = \frac{E_0 \, \beta \, \gamma}{c}.$$

With the injection energy from the non-relativistic region ( $\gamma \approx 1$ ) and unchanged particle revolution frequency ( $\beta_d = \beta_p$ ), expression (9) becomes simpler:

$$k \sim E_0, \tag{10}$$

i.e., the maximum density of a deuteron beam in a bunch will be twice as large.

For relativistic injection energies  $(E \approx Pc)$  and the same magnetic rigidity  $(P_d = P_p)$  we obtain

$$k \sim \frac{1}{E_0^2},\tag{11}$$

which decreases the maximum density of the deuteron beam by a factor of four.

However, it is not always possible to satisfy the condition  $\dot{\beta}_d = \beta_p$  or  $P_d = P_p$ . In this case (9) is transformed to

$$k \sim \frac{EB_i^2}{E_0^2},\tag{12}$$

where  $B_1$  is induction in dipoles at injection. From (12) a possibility of an intermediate variant between (10) and (11) follows. Longitudinal effects under the phase stability, as a rule, do not impose additional limitations on the beam charge density.

2.5. Maximum vacuum in a chamber. The multiple Coulomb scattering effects in annular accelerators for protons and deuterons can be compared by the root-mean-square increase in the amplitude of betatrom oscillations. At a fixed length of the closed orbit, the same dynamic characteristics  $(Q_r, Q_z)$  and vacuum for this relation can be written as [9]

$$\langle a^2 \rangle \sim \frac{\mathcal{Q}}{P\beta^2},$$
 (13)

where  $\mathcal{L} = L_{e0}\nu$ ,  $\nu$  is the number of revolutions necessary to double the injection (kinetic) energy, P and  $\beta$  are taken at the injection energy.

If the equality  $P_d = P_p$  is observed in injection, then at the non-relativistic energy it follows from (13) that  $\langle a_d^2 \rangle = 2 \langle a_p^2 \rangle$  owing to a decrease in the deuteron velocity at injection and a decrease in the number of revolutions at energy doubling for the same energy gain per revolution.

In a relativistic case with  $P_d = P_p$  or for non-relativistic energy at  $\beta_d = \beta_p$  at it jection, it directly follows from (13) that  $\langle a_d^2 \rangle = \langle a_p^2 \rangle$ .

Within this model of scattering by residual gas, the distribution over amplitudes of betatron oscillations follows the Raleigh law:

$$F(a) = \frac{a}{\langle a^2 \rangle} e^{-\frac{a}{2\langle a^2 \rangle}}.$$
 (14)

Thus, for injection with  $P_d = P_p$ , only the non-relativistic part of the complex must be checked for multiple scattering effect in transition from a proton to a deuteron beam.

2.6. Lurrinosity. One can estimate the luminosity (L) for deuterons assuming that the root-mean-square dimensions of beams at collision points, revolution frequencies of particles and the number of bunches in a circulating beam are the same for both variants. In this case we have

$$L \sim N^2, \tag{15}$$

where N is the number of particles in a circulating beam.

#### 3. Estimation of Deuteron Mode Parameters

Proceeding from the considerations of section 2 we shall estimate parameters of UNK operation in the deuteron mode. The results are given in the table compared with the proton variant. For deuterons, there are only values of those parameters that differ from the proton variant.

The energy of injection into booster was calculated with the given minimum revolution frequency of protons  $f_p = 0.7467$  MHz. Thus, the field induction at injection could be found from (1) and (2). The maximum number of particles in a circulating beam, determined by the shift of the frequency of axial free oscillations due to Coulomb repulsion, can be calculated in accordance with (9) by the formula [10]

$$N_{d} = \frac{r_{p}}{r_{d}} \frac{\gamma_{d}(\gamma_{d}^{2} - 1)}{\gamma_{p}(\gamma_{p}^{2} - 1)} \frac{f_{d}}{f_{p}} N_{p}, \tag{16}$$

Table

LINAC	Protons	Deuterons
Output energy (MeV)	30	60
Current pulse amplitude (mA)	67	76
BOOSTER	Protons	Deuterons
Final energy (kinetic) (GeV)	1.5	1.05
Intensity in pulse (particles/cycle)	9x10 <sup>11</sup>	1.0x10 <sup>12</sup>
Circulating current (mA)	425	483
Transition energy (kinetic) (GeV)	2.55	5.096
Magnetic field induction in injection (T)	0.139	0.278
Frequency variation range (MHz)	0.747—2.79	0.747—2.32
U-70	Protons	Deuterons
Final energy (kinetic) (GeV)	70	69
Intensity in cycle (particles/cycle)	1.1x10 <sup>13</sup>	1.2x10 <sup>13</sup>
Circulating current (mA)	357	405
Transition energy (total) (GeV)	8.876	17.738
Frequency variation range (MHz)	5.56—6.1	4.666.06
UNK-I and UNK-II (collider mode)	Protons	Deuterons
C.m.energy (TeV)	2.2	2.19
Full required intensity (particles/cycle)	2.4x10 <sup>14</sup>	6x10 <sup>13</sup>
Circulating current (mA)	554	139
Luminosity (cm <sup>-2</sup> s <sup>-1</sup> )	1x10 <sup>32</sup>	6x10 <sup>30</sup>
Transition energy (GeV)	42	84
UNK-I	Protons	Deuterons
Maximum energy (GeV)	600	599
collider mode	400	399
Planned intensity (particles/cycle)	6x10 <sup>14</sup>	1.5x10 <sup>14</sup>
Circulating current (mA)	1385	347
UNK-II	Protons	Deuterons
Maximum energy (GeV)	3	3
Planned intensity (particles/cycle)	6x10 <sup>14</sup>	1.5x10 <sup>14</sup>
Circulating current (mA)	1385	347
UNK-II and UNK-III (collider mode)	Protons	Deuterons
C.m.energy (TeV)	6	6
Full required intensity (particles/cycle)	2.4x10 <sup>14</sup>	6x10 <sup>13</sup>
Luminosity (cm <sup>-1</sup> ·s <sup>-1</sup> )	$2.8 \times 10^{32}$	1.7x10 <sup>31</sup>

where  $r_p$  and  $r_d$  are the classical radii of the proton and deuteron. It is assumed that the permissible frequency shift, beam emittance and bunching factor are the same in both cases. The estimation was done with the energy of injection in the facility. The decisive factor for the beam intensity in the whole chain of accelerators of the complex (linac, booster, U-70, UNK-I, UNK-II) is the maximum number of particles attained in U-70 now. Yet, after the updating of U-70 an almost 5-fold increase in the number of ejected beam particles is expected. This fact was taken into account in calculation of deuteron intensities given in the table. It was also assumed that the efficiencies of acceptance, transmission, re-bunching (U-70) and beam extraction are the same for protons and deuterons and have the values achieved at present.

The intensity of the circulating beam is

$$I_c = \frac{eNf_{rf}}{q},\tag{17}$$

where q is the ratio of the accelerating field frequency  $f_{rf}$  to the particle revolution frequency.

As the given magnetic rigidity of the rings  $(B\rho)$  one determines the final energy of accelerators in accordance with (1), the revolution frequency by (4) and the transition energy by (8). A new thing, as compared with the proton variant, is the transition energy in the range of UNK-I energies in acceleration of deuterons. The methods of overcoming the transition energy were mentior ed in section 2.

The centre-of-mass (c.m) energy of colliding beams was estimated by the well-known formula [11]:

$$E_{\rm c m.} = c^2 \sqrt{[m_{01}^2 + m_{02}^2 + 2m_{01}m_{02}\gamma_1\gamma_2(1 - \beta_1\beta_2)]}, \tag{18}$$

where  $m_{01}$ ,  $m_{02}$  are the rest masses of particles;  $\beta_1$ ,  $\beta_2$  are taken algebraically i.e., with their signs.

The dynamic characteristics of the transverse motion of deuterons (interval frequencies, envelopes, etc.) in the accelerating chain from the booster to UNK-I are fully equivalent to the proton mode characteristics. So, with the same emittance of proton and deuteron beams injected from the linear accelerator and with the deuteron intensity at which the Coulomb shift of betatron frequencies is equal to or smaller than for protons, the transverse emittance of the deuteron beam and the acceptance of the accelerators of the complex can surely be matched.

#### 4. Technical Realization

As seen from the aforesaid, the deuteron mode of the UNK operation is possible with the existing and planned equipment without essential changes.

The only facility to be built is a linear accelerator for deuterons to inject them in the booster. As is known, however, while making U-70 into an injector of the UNK, one intends to increase the injection energy from 30 MeV to 60 MeV [12]. To this end, a new linear accelerator is supposed to be built. While the new accelerator, one could take into account the requirements imposed by the deuteron mode and experience of IHEP in designing a heavy-current linear accelerator for deuterons [13].

Besides, it is necessary to allow for a system for overcoming the transition energy in the UNK-1. The final considerations for selection of its parameters will be formulated later in the course of elaboration of this proposal.

#### 5. Conclusion

The deuteron mode of acceleration can be regarded as the initial step of the programme for acceleration of ions heavier than hydrogen at the UNK.

Implementation of this programme will require development of the necessary ion sources and upgrading of several systems of the complex, especially the injection section, the beam indication system and some others. Suitability of this programme and the rate of its implementation will depend of the experiments proposed with allowance for the status of ion acceleration activity at large accelerating complexes in European centres and in the USA. We think that it will be undoubtedly useful to develop the relevant techniques and technologies in advance.

### 6. Acknowledgment

We gratefully acknowledge help and support of Logunov A.A.

#### References

- 1. Ageev A.I. Accelerator-Storage Complex of IHEP. In: Proc. of 10th All-Union Conf. on Charged Particle Accelerators, JINR D9-87-105, Dubna, 1987, v.2, p.430.
- 2. Kapchinsky l.M. et al. In: Proc. of 11th All-Union Conf. on Charged Particle Accelerators, JINR 9-89-52, Dubna, 1989, v.1,p.37.
- 3. Aleev E.A. et al. In: Proc. of 9th All-Union Conf. on Charged Particle Accelerators, Dubna, 1985, v.1, p.14.

- 4. Baldin A.M. et al. JINR P9-5442, Dubna, 1970.
- 5. Azo Yu M. et al. In: Proc. of 8th All-Union Conf. on Charged Particle Accelerators, Dubna, 1983, v.1, p.212.
- 6. Vladim rsky V.V. et al. Proton Synchrotron on Energy 60—70 GeV. In: Proc of Int. Conf. on Accelerators, Moscow, 1964, p.197.
- 7. Myae E.A., Pashkov P.T. In: Proc. of 8th All-Union Conf. on Charge 1 Particle Accelerators, Dubna, 1983, v.1, p.231.
- 8. Trboevic D. Design Method of High Energy Accelerator without Transition Energy. In: Proc. of 2nd European Particle Accelerator Conference, Nice, France, Editions Frontieres, 1980, v.11, p.1536.
- 9. Blachman N., Courant E. Rev. Sci. Intsr., 1953, 24, p.836.
- 10. Kolomensky A.A. Physical Bases of Methods of Charged Particles Accelerations. Moscow, 1980, p.249.
- 11. Bovet C. et al. Selection of Formulae and Data Useful for the Design of A.G. Synchrotrons, CERN, 1970, p.6.
- 12. Gurevich A.S. et al. Upgrading 70 GeV IHEP Accelerator as UNK Injector, in Proc. of 2nd European Particle Accelerator Conference, Nice, France, Editions Frontieres, 1980, v.1, p.415.
- 13. Budanov U.A. et al. IHEP, 90-126, Protvino, 1990.

## EXPERIMENTAL STUDY OF SUPERNEUTRON-DEFICIENT TIN ISOTOPES

M.Lewitowicz<sup>1</sup>, R.Anne<sup>1</sup>, G.Auger<sup>1</sup>, D.Bazin<sup>1</sup>, M.G.Saint-Laurent<sup>1</sup>, R.Grzywacz<sup>2</sup>, M.Pfützner<sup>2</sup>, K.Rykaczewski<sup>2</sup>, J.Zylicz<sup>2</sup>, S.Lukyanov, A.Fomichov, Yu.Penionzhkevich, O.Tarasov, V.Borrel<sup>3</sup>, D.Guiillemaud-Mueller<sup>3</sup>, A.C.Mueller<sup>3</sup>, H.Keller<sup>3</sup>, O.Sorlin<sup>3</sup>, F.Pougheon<sup>3</sup>, M.Huyse<sup>4</sup>, T.Pluym<sup>4</sup>, J.Szerypo<sup>4</sup>, J.Wauters<sup>4</sup>, C.Borcea<sup>5</sup>, K.Schmidt<sup>6</sup>, Z.Janas<sup>6</sup>

Fragmentation reactions analyzed by means of the projectile fragment separator LISE3 at GANIL were exploited to enable the nuclei in the closest neighbourhood of <sup>100</sup>Sn to be identified and their decay properties studied. Preliminary results of the first experiments performed with the <sup>112</sup>Sn beam are presented. The first identification of <sup>102</sup>Sn and confirmation of an existence of <sup>101</sup>Sn open new possibilities in the study of nuclei close to <sup>100</sup>Sn.

The joint investigation has been performed at GANIL by the collaboration LNR — GANIL — Warsaw University.

## Эксперименты по синтезу супернейтронодефицитных ионов олова

## М.Левитович и др.

Описываются результаты экспериментов по определению стабильности ядер вблизи дважды магического <sup>100</sup>Sn. Для этого использоваль сь реакции фрагментации ионов <sup>112</sup>Sn, ускоренных на ускорителе ГАНИЛ. Сепарация и идентификация полученных фрагментов осуществлялись на фрагмент-сепараторе LISE3. Впервые идентифицированный изотоп <sup>102</sup>Sn и подтверждение существования <sup>101</sup>Sn открывают новую возможность в исследовании ядер, близких к <sup>100</sup>Sn.

Работа выполнена в GANIL коллаборацией ЛЯР — GANIL — Варшавский университет.

<sup>&</sup>lt;sup>1</sup>GANIL, Caen, France

<sup>&</sup>lt;sup>2</sup>Warsaw University, Poland

<sup>&</sup>lt;sup>3</sup>IPN, Orsay, France

KU, Leuven, Belgium

<sup>&</sup>lt;sup>5</sup>IAP, Bucharest, Romania <sup>6</sup>GSI, Darmstadt, Germany

#### 1. Motivation

Studies of doubly-closed-shell and neighbouring nuclei are obviously important for testing and further development of nuclear models. Such studies of ruclei far from stability [1] have additionally an astrophysical context. Reliable predictions of nuclear structure and disintegration rates, especially for the Gamow — Teller (GT) beta decay, are crucial for understanding the nucleosynthesis scenarios under stellar conditions. In case of neutron-deficient nuclei these scenarios include the rapid proton-capture process.

These remarks may be considred as a general motivation for our interest, and the interest of several other experimental and theory groups, in the  $^{100}$ Sn region. Let us recall that  $^{100}$ Sn is the yet unidentified isotope of tin with a deficit of about 18 neutrons with respect to the line of beta stability. It is the heaviest Z = N doubly magic nuclear system that one may hope to reach in experiment (the next one would be  $^{164}$ Pb, presumably well beyond the proton-drip line). With the shell-model energy gap, that may be here as high as  $6.5 \, \text{MeV}$ , the closed-shell properties of  $^{100}$ Sn are expected to be well pronounced.

The shell model picture of the beta decay in the  $^{100}$ Sn region is extremely simple. This decay is strongly dominated by one channel, the  $\pi g_{9/2} \rightarrow \nu g_{7/2}$  GT transformation. Hence, interpretation of experimental data can be particularly unambiguous, a very important feature for testing nuclear models and an insight into the problem of the GT strength quenching.

The large distance of  $^{100}$ Sn from the line of stability is reflected in the decay energy  $Q_{EC}$  which is predicted to be 7 to 8 MeV. For some of the neighbouring nuclei, the  $Q_{EC}$  values should be even higher. A large fraction of the total GT strength can be observed. Beta-delayed proton emission becomes possible. This proton emission is strongly related to the properties of the GT decay. For odd-A and odd-odd parent nuclei, most of the beta strength is associated with the transformation of a  $g_{9/2}$  proton from the even-even core. The relevant GT transitions lead to multiparticle configurations at high excitation energies. This opens a possibility for emission of protons with a detectable yield. In fact, due to law background, measurements of proton spectra can be the best way for an identification and/or GT decay study of nuclei very far from stability.

The decay of nuclei in the <sup>100</sup>Sn region has been investigated in several experiments on beta decay using the on-line mass-separators at GSI Darm-

stadt, ISOLDE CERN and LISOL Leuven. However, <sup>100</sup>Sn has not been discovered. Progress towards this nucleus using on-line mass-separator based studies is made very difficult by a drastic decrease of the production cross-section in both spallation and heavy ion fusion-evaporation reactions. The yield is further reduced by the small overall release efficiency caused by the short half-lives of investigated nuclei. Obviously, new production methods and separation techniques have to be tested in order to cross the border line of known nuclei (see the next section).

Therefore we proposed [2] studies of the nuclei in the <sup>100</sup>Sn region using the fragmentation reactions and LISE3 projectile fragment separator at the GANIL facility. It was expected that, relative to earlier experiments, production yields of the most neutron-deficient nuclides will be increased, and the limit for detectable half-lives will be essentially improved. These two improvements offer an opportunity to reach <sup>100</sup>Sn. The expected increase of the production yields is mainly due to the use of <sup>112</sup>Sn as a projectile. This rare primary beam is developed at GANIL in a close and already very fruitful collaboration with the Laboratory of Nuclear Reactions, JINR at Dubna.

## 2. Border Line of Known Nuclei near 100 Sn

A section of the chart of nuclei near  $^{100}\rm{Sn}$  is displayed in Fig.1. The last decays with unambiguously measured half-life in the vicinity (Z  $\leq$  50) of  $^{100}\rm{Sn}$  are those of  $^{103}\rm{Sn}$  ( $T_{1/2}=7\pm1.5\,\rm{s}$ ),  $^{100}\rm{In}$  ( $T_{1/2}=3.5\pm0.7\,\rm{s}$ ) and  $^{98}\rm{Cd}$  ( $T_{1/2}=9.2\pm0.3\,\rm{s}$ ).

The proton shell closure at Z=50 creates a favorite energy conditions for alpha and proton emission from the ground-state of neutron-deficient tellurium (Z=52) and antimony (Z=51) isotopes, respectively. Indeed, an island of alpha emitters above tin has been found experimentally including the lightest one known so far —  $^{106}$ Te. Recently, the Berkeley group presented an evidence for the ground-state proton decay of  $^{105}$ Sb [4].

## 3. Experiment

In the experiment performed at GANIL (26 Oct. — 4 Nov., 1993) we used <sup>112</sup>Sn<sup>43+</sup> beam at 58 MeV/nucleon impinging on a 78 mg/cm<sup>2</sup> thick <sup>nat</sup>Ni target. The mean intensity of the primary beam was about 130 enA

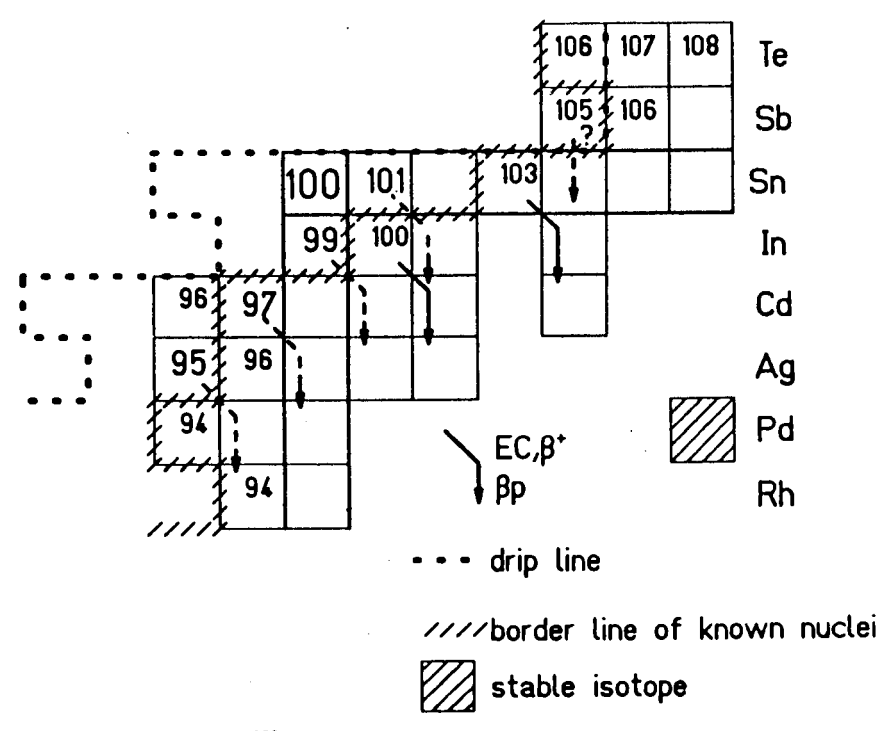


Fig.1. Nuclides near  $^{100}$ Sn known in June 1993 [2]. At present, one has to add  $^{94,95}$ Ag and  $^{101}$ Sn [3],  $^{103}$ Sb [4] and  $^{102}$ Sn — this work

and it was limited by the data acquisition system. The choice of the nickel target enhances a transfer-type reaction. This in particular increases in an important way production of the nuclei with Z > 50. A  $9.5 \, \text{mg/cm}^2$  thick carbon foil placed just behind the target decreased a width of the charge state distribution in this way that about 90% of all tin isotopes were produced in the 48+ and 49+ charge states.

The experimental device used to select the exotic nuclei was the LISE3 spectrometer [5]. Briefly described, LISE3 is a doubly achromatic system providing selection of reaction products following the ratio  $A\nu/Q \sim B\rho$ , where A, Q and  $\nu$  are, respectively, the mass, the ionic charge and the velocity of the ions and  $B\rho$  is the magnetic rigidity of the spectrometer. The Wien filter placed at the end of the spectrometer allows for an additional velocity selection of the reaction products. In order to have a good velocity determination and to decrease the counting rate we reduced the momuntum acceptance of LISE to  $\pm$  0.1%.

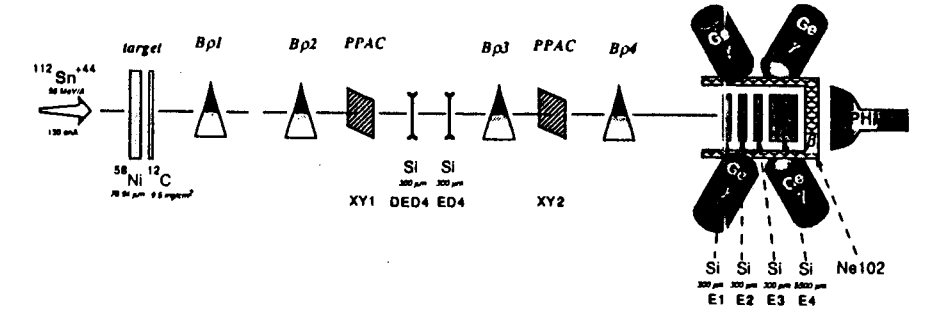


Fig. 2. Schematic view of the experimental set-up

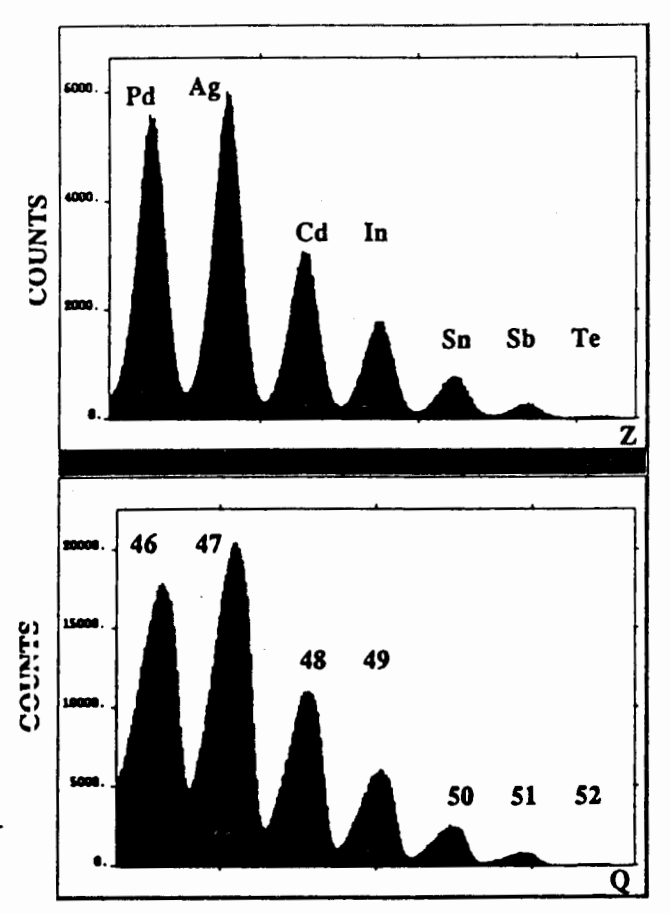
A schematic view of the experimental set-up used in the present study is shown in Fig.2. All selected nuclei were stopped at the last image point of the spectrometer in a four-member silicon detector telescope (E1, E2, E3, E4) providing energy-loss ( $\Delta E$ ) and total-kinetic-energy (TKE) measurements. Furthermore, we measured the  $B\rho 1$  and  $B\rho 2$  values of the dipoles with a nuclear magnetic resonance probes, and the time-of-flight (TOF) between the target and the telescope, the start signal being given by the first silicon detector E1, and the stop by the radiofrequency of the last GANIL cyclotron. Two removable silicon detectors DED4 and ED4 and two removable position-sensitive avalanche counters XY1 and XY2 were used for a fine tuning of reaction products along the LISE spectrometer. Four big (80—90%) germanium detectors and a NE102 plastic scintillator surrounding the final telescope served for measurements of beta and gamma radiation coming from the nuclei implanted in the silicon detectors.

## 4. Data Analysis and Results

The analysis of the experimental data aims at a correct identification of all nuclei selected by the spectrometer. The atomic number is determined by a combination of the energy loss  $\Delta E$  and time-of-flight (TOF) measurements according to the Bethe formula:

$$Z \sim \sqrt{\Delta E / \left(\frac{1}{\beta^2} \ln \left(\frac{5930}{1/\beta^2 - 1}\right) - 1\right)}.$$
 (1)

The determination of Z used to calibrate this formula is done using the primary beam (Z = 50) and by taking into account cross-checks such as the non-existence of <sup>8</sup>Be on the A/Q = 2 line and other equal-A/Q alignments.



F g.3. Atomic-number and charge-state distributions obtained from the experimental data at  $B\rho=1.98835$  Tm with the use of formulae ( ) and (2), respectively

The Z spectrum obtained in the experiment for a tin region in presented in an upper part of Fig.3.

The charge state Q of each isotope can be calculted from the relativistic formula:

$$Q = 3.33 \cdot 10^{-3} \frac{\text{TKE } \beta \gamma}{B \rho (\gamma - 1)}, \qquad (2)$$

where the TKE has dimensions of MeV.

The TKE is calculated as a sum of energy losses in each silicon detector. A very careful energy calibration of E1, E2, E3 and E4 detectors was done

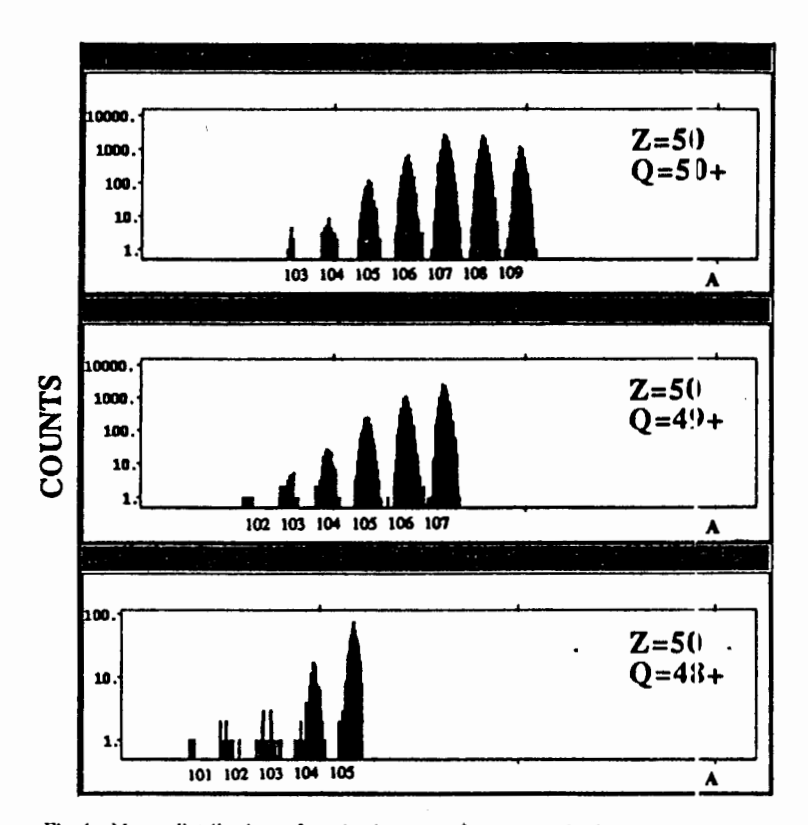


Fig.4. Mass distributions for tin isotopes for selected charge states Q at  $B\rho=1.98835\,\mathrm{Tm}$ 

using the primary  $^{112}$ Sn beam of five different energies. This calibration, which is valid in the energy region corresponding to the expected TKE for nuclei around A = 100, takes into account nonlinear effects in the electronic chains and the silicon detectors themselves.

Once the charge state has been identified, the mass A of each nucleus expressed in a.m.u. can be extracted from the equation:

$$A = \frac{B\rho Q}{3.105 \,\beta\gamma} \,. \tag{3}$$

Since the charge resolution was sufficiently good (see a lower part of Fig.3), it was possible to improve the mass resolution by forcing integer values for Q. These integers were assigned for tin isotopes by putting the  $\Delta Q = 0.5$  wide windows on the Q = 50+, 49+ and 48+ charge states. The resulting mass distributions for selected Q values are shown in Fig.4. In the

distributions corresponding to Q = 49+ and Q = 48+, the events from  $^{102}$ Sn are clearly visible. It is a first observation of this tin isotope. In the second of these distributions, four events due to  $^{101}$ Sn are present.

The above results were obtained at  $B\rho=1.98835$  Tm which was chosen after test measurements performed at several  $B\rho$  values. The above spectra represent statistics obtained after about 30 hours of measurement with a mean intensity of primary beam of about 80 enA.

The complete data evaluation which includes the analysis of beta-gated gamma spectra, is in progress.

#### 5. Conclusions

The first GANIL experiment with the <sup>112</sup>Sn beam, aiming at an identification and studies of nuclei near <sup>100</sup>Sn, brought promising results and an important experience. With this experience, after an upgrading of the experimental set-up (adding SISSI solenoids right after the CSS2 and a new dipole magnet at the end of LISE3), there will be a good change to identify <sup>100</sup>Sn unambiguously and to start the decay spectroscopy in this region of highly neutron-deficient nuclei.

The experience gained during such studies and the detection equipment which will be developed will also be used at the Warsaw Heavy-Ion Cyclotron Laboratory coming into operation in 1994 and also in the future Radioactive Nuclear Beam ISOL-type facility (SPIRAL).

#### References

- 1. Proceedings of the Sixth NFFS and the Ninth AMCO Conference, Bernkastel-Kues, Germany, 19—24 July, 1992, Edited by R. Neugart and A. Wohr, IOP, Bristol, 1992.
- Rykaczewski K. et al. Towards the Study of Gamow Teller Beta Decay of <sup>100</sup>Sn, Proposal for the GANIL Experiment E226, June 1993.
- 3. Roeckl E. Nachrichten GSI 09-93.
- 4. Tighe R.J. et al. Preprint LBL-34510, Berkeley, August 1993.
- 5. Anne R., Mueller A.C. Nucl. Instr. Meth., 1992, B70, p.276. and references therein.

Received on January 10, 1994.